Modeling and Simulation of Air Conditioner Motors and Investigation of Cascaded Stalling

by

Chaitanya A. Baone

A thesis submitted in partial fulfillment of the

requirements for the degree of

Master of Science

(Electrical Engineering)

at the

UNIVERSITY OF WISCONSIN-MADISON

2009

APPROVED

By

Advisor: Professor Ian A. Hiskens

Date: December 18, 2009

Abstract

Air conditioner (A/C) motor stalling is considered as one of the main reasons for the occurrence of delayed voltage recovery events leading to voltage collapse. In recent years, the phenomenon of Fault-Induced Delayed Voltage Recovery (FIDVR) has increasingly been observed. Planning tools have been found inadequate to capture FIDVR-type events, primarily due to inaccurate modeling of A/C motor loads. A dynamic A/C motor model based on the phasor modeling approach is considered in this work. The model accurately represents the behavior of A/C motors during and after a fault. Sensitivity analysis is performed to arrive at a set of more significant model parameters. This information may be used effectively in tuning the model parameters for various types of A/C motors.

The next step in the development of a load model capable of accurately capturing the dynamical behavior of loads in the system is the aggregate modeling of several A/C motors. Instead of using a simplistic method of aggregating these machines into a single equivalent machine based on their ratings, an analytical approach based on bifurcation theory is presented in this work. The method characterizes the stalling behavior of several A/C motors in the system based on the system voltage level and thus provides a way for a more refined approach to aggregate A/C motor modeling.

Acknowledgements

I want to thank my advisor, Professor Ian Hiskens, for giving me the opportunity to pursue this research under his supervision. I want to thank him for his invaluable guidance throughout the duration of my course.

I also want to thank Professor Bernie Lesieutre for his constant guidance and support over the entire duration of this thesis. I am deeply indebted to him for all the fruitful and enlightening discussions.

I want to thank Professors Christopher DeMarco, B. R. Barmish, and Giri Venkataramanan for the courses they taught me and helped me understand some of the concepts and tools required to pursue research in the area of power systems. I also want to thank Steve Almquist and Bo Gong for all their help with understanding the DAIS framework. I want to thank my friends at UW-Madison, Nidhishri Tapadia, Shreesha Srinath, and all the members of the power systems group at UW-Madison for making this experience memorable and enjoyable.

Last, but certainly not the least, I want to thank my family – Aai, Baba, and Dada for encouraging me to pursue higher studies and for their constant support and affection over the years.

Table of Contents

List of Figures

Introduction

The on-going changes in the electric power industry are resulting in new features of power systems, which are characterized by complex interconnections and the utilization of a large variety of controllers for optimizing the system operation and the use of the available resources. Moreover, with the deregulation of utilities, the power networks are understood to be channels for transfer of electricity from points of production to points of consumption, depending on a competitive system based on time varying prices. The complexity of the system, the nature of the dynamics that affect it and the external factors interacting simultaneously require special attention in order to provide a properly operated and designed power system. Modeling the system elements forms an important aspect of proper power system planning and operation. Detail models exist for the generation and transmission system elements. However, loads are often not modeled accurately. One reason for this is the inherent uncertainty involved in modeling the system load, as one can never accurately predict how the load would look like at any point in time in the future. However, there is also a lack of understanding of the characteristics of certain critical loads in the system and so the resulting load model often does not accurately capture the inherent nature of the load. There is also the issue of computational complexity, since it is not feasible to model each and every element of the system load while performing simulation studies.

Recently, there has been an increasing concern with regard to air conditioner (A/C) motor load operation in the system. A/C motors form a significant portion of the system

load. It has been found that stalling of A/C motors in the event of a system fault may lead to delayed voltage recovery, which may potentially lead to a voltage collapse.

A delayed voltage recovery event, or more popularly known as a Fault-Induced Delayed Voltage Recovery (FIDVR) event, is the phenomenon whereby system voltage remains at significantly reduced levels for several seconds after a transmission, sub-transmission, or distribution fault has been cleared. A severe event can result in fast voltage collapse. FIDVR is caused by highly concentrated induction motor loads with constant torque which stall in response to low voltages associated with system faults and draw excessive reactive power from the grid. FIDVR is worst when there is a concentration of "stall-prone" motors in a region. Not all motors are vulnerable to stalling. For example, large industrial motors often have contactors that will drop the motor out during voltage dips, thus limiting the negative impact of these motors. Large HVAC units may also have motor protection that will trip the unit offline before stalling occurs. Smaller HVAC units, however, may not have protection that will trip the unit off before stalling occurs. FIDVR events become increasingly probable with continuing market penetration of high efficiency low inertia air conditioning loads.

Once the A/C motor stalls in the event of a fault, it remains stalled in majority of the cases even if the voltage recovers, as the compressor is unable to restart against the full head of pressure. It takes one to five minutes before pressure is equalized so that the motor can restart [1]. In the stalled condition, the motor typically requires 5-6 times its steady-state current with the result that system voltage can be significantly depressed for seconds after the

fault is cleared further aggravating the initial fault voltage depression. As a result, additional induction motors can slow down and stall and create a voltage cascade.

Planning studies have not been able to simulate FIDVR events very accurately due to inaccurate modeling of A/C motor loads. Uncorrected, this modeling deficiency has a two-fold detrimental effect. First, it can result in studies that do not adequately identify potential FIDVR events. Second, it can give false confidence in mitigation plans designed to prevent reoccurrence of events.

There have been a number of incidents of delayed voltage recovery or voltage collapse following a major transmission system disturbance on several utility systems in recent years. Some of these incidents are described in detail in [2, 3, 4]. In all these cases, post-incident analyses have attributed these incidents to the increased reactive power demand of stalled A/C motor loads under reduced voltage conditions and the lack of adequate dynamic reactive power support in the system.

Another question that arises while deciding on an accurate load model to capture the behavior of several such components is that of aggregation. The simplistic approach that is adopted in most studies is to aggregate all the individual motor models in a sufficiently large area into a single equivalent motor model at a particular bus. The key characteristic of the air conditioner motors is their stalling behavior. An aggregate model that combines several air conditioner units into a single unit is bound to lose key information about the stalling characteristics of these machines and lead to inaccurate composite load modeling.

In this thesis, a detailed model for A/C compressor motors is considered. The model is based on the dynamic phasor modeling approach developed by B. Lesieutre in [1]. The

model is dynamic in nature and accurately captures the relations between voltage, frequency, active power, and reactive power. The model simulations show the typical behavior of these machines in the event of a fault resulting in delayed voltage recovery. The differential-algebraic impulsive switched (DAIS) modeling framework for power system simulation developed by I. Hiskens [5, 6] is used to simulate the A/C motor model. Furthermore, sensitivity analysis on the A/C motor model is performed to arrive at the set of more significant model parameters. The other part of this thesis is directed towards investigating cascaded stalling of air conditioners and using this information to come up with a better structure for aggregate A/C motor load modeling.

Outline of Text by Chapter

Chapter 1 presents a brief literature review of load modeling in power systems, FIDVR modeling efforts and bifurcation analysis in power systems.

The A/C motor model using the dynamic phasor modeling approach is presented in chapter 2. The DAIS framework used to simulate the system and to perform sensitivity analysis is also briefly discussed. Simulation results of the model are presented along with results of sensitivity analysis to arrive at the more sensitive model parameters.

Chapter 3 presents a continuation method based on the predictor-corrector approach adopted to investigate cascaded stalling of A/C motors. A system consisting of two phasor modeled A/C motors connected to a voltage source through a feeder is considered and the results of the continuation method applied to this system are presented.

Chapter 4 includes a concluding summary and recommendations for future work.

Chapter 1 Literature Review

1.1 Load Modeling in Power Systems

The power system engineer bases decisions concerning system reinforcements and system performance in large part on the results of power flow and stability simulation studies. Representation inadequacies that cause under or over building of the system or degradation of reliability could prove to be costly. In performing power system analysis, models must be developed for all pertinent system components, including generating stations, transmission and distribution equipment and loads. Much attention has been given to models for generation and transmission and distribution equipment. The representation of loads has received less attention and continues to be an area of greater uncertainty. Many studies have shown that load representation can have significant impact on analysis results [7, 8]. Loads for voltage stability analysis are typically represented as a combination of static and dynamic loads. Some of the commonly used static load models are as follows:

1. Constant impedance load model is a static load model where the power varies directly with the square of the voltage magnitude. It may also be called a constant admittance load model.

2. Constant current load model is a static load model where the power varies directly with the voltage magnitude.

3. Constant power load model is a static load model where the power does not vary with changes in voltage magnitude. It may also be called constant MVA load model. Because constant MVA devices, such as motors and electronic devices, do not maintain this

characteristic below some voltage (typically 80 to 85%), many load models provide for changing constant MVA load model to constant impedance load model or tripping the load below a specified voltage.

4. Polynomial load model is a static load model that represents the power relationship to voltage magnitude as a polynomial equation, usually of the form,

$$P = P_o\left[a_1\left(\frac{V}{V_o}\right)^2 + a_2\left(\frac{V}{V_o}\right) + a_3 \right] \quad (1.1)$$

$$Q = Q_o\left[a_4\left(\frac{V}{V_o}\right)^2 + a_5\left(\frac{V}{V_o}\right) + a_6 \right] \quad (1.2)$$

Where,

V is the bus voltage magnitude,

P and Q are the active and reactive powers consumed by the load respectively,

V_o , P_o and Q_o are the nominal operating values for V, P and Q respectively.

The parameters of this model are the coefficients a_1 to a_6 and the power factor of the load. This model is sometimes referred to as the "ZIP" model, since it consists of the sum of constant impedance (Z), constant current (I) and constant power (P) terms.

5. Exponential load model is a static load model that represents the power relationship to voltage as an exponential equation, usually of the form,

$$P = P_o\left(\frac{V}{V_o}\right)^{np} \quad (1.3)$$

$$Q = Q_o\left(\frac{V}{V_o}\right)^{nq} \quad (1.4)$$

The parameters of this model are the exponents np and nq, and the power factor of the load. By setting these exponents to 0, 1, or 2, the load can be represented by constant power, constant current or constant impedance models respectively. Other exponents can be used to represent the aggregate effect of different types of load components. Exponents greater than 2 or less than 0 may be appropriate for some types of loads.

6. Frequency-dependent load model is a static load model that includes frequency dependence. This is usually represented by multiplying either a polynomial or an exponential load model by a factor of the form,

$$\left[1 + a_f\left(f - f_o\right)\right] \tag{1.5}$$

Where,

f is the frequency of the bus voltage,

f_o is the rated frequency and a_f is the frequency sensitivity parameter of the model.

The most commonly accepted static load model represents active power as constant current, and reactive power as constant impedance [7]. The constant current model for active power stems from the resistive nature of heating and lighting loads and the characteristics of motor loads. The constant impedance representation of reactive power results from the leakage and magnetizing reactance of transformers and motors, and power factor correction capacitors. Constant impedance, current and power (ZIP load model) static load models with algebraic equations using coefficients for different types of loads have also been used for steady-state voltage stability analysis [9, 10]. Some of the other modeling techniques in the literature of power system load modeling are also briefly discussed here.

A modeling technique based on real system data is presented by the authors in [11]. This technique is based on genetic algorithm (GA). Different from conventional optimization techniques, genetic algorithm is a population-based algorithm. The population of all possible solution sets is generated in a stochastic manner and the best found solution set acts as parents for successive generations. The authors propose an equivalent area load model and to optimize the parameters of this model, an improved GA is presented. Simulation results show that this method is capable of finding a precise model for the load area in a particular power system. The model presented in this paper is a polynomial load model and does not address the dynamic aspects of loads.

The authors in [12] present a non-linear dynamic load model using GA. The authors develop a composite dynamic static model (CDSM), which includes the effect of voltage angle on transient active power. They use GA for the estimation of parameters. The GA based parameter estimation approach is successfully applied to induction motor models, input output models and neural network models.

The authors in [13] propose an approach to dynamic load modeling. They use a constrained non-linear recursive filter (CNLRF) for parameter estimation, which is based on data obtained from field tests. A power system may consist of different types of complex loads with different characteristics. To aggregate these different types of loads and to represent them in the form of equivalent models is important with regard to the modeling and analysis of the system. Induction machines are major loads in any power system in most of the cases. There are two approaches for the aggregation of induction motors; one is theoretical aggregation, and the other is identification aggregation. Theoretical aggregation

requires the parameters of all individual loads and transmission and distribution lines, which is not practically feasible. Identification aggregation methods are based on the least square parameter estimation algorithm and require iterative solution of the state equations. The authors suggest an improved method of identification aggregation for the dynamic load model, which identifies model parameters based on the input-output information of the system without resorting to iterative solution of the state equations.

The main limitation of the static load model is that it does not represent the increased active and reactive power demands of motor loads under reduced voltage conditions (due to the motors slowing down), as well as the behavior of stalled motor loads.

1.2 Fault-Induced Delayed Voltage Recovery

The North American Electric Reliability Corporation (NERC) Transmission Issues Subcommittee provides the following definition for FIDVR in their recently published white paper [14]:

Fault-Induced Delayed Voltage Recovery — a voltage condition initiated by a fault and characterized by:

- Stalling of induction motors
- Initial voltage recovery after the clearing of a fault to less than 90% of pre-contingency voltage
- Slow voltage recovery of more than 2 seconds to expected post-contingency steady-state voltage levels.

Recently, some people have contributed towards trying to accurately model FIDVR-type events. The authors in [15] propose an aggregate load model that includes induction

motors, static constant current and constant impedance load models. They consider the distribution of loads as 50% small induction motor loads and 50% static loads. They validate their model based on actual events observed during 1999 and 2006 in the southern control area. Their model replicates delayed voltage recovery in the event of a fault. The model is developed using the standard PSS/E models. They mention that their model does not fully capture stall characteristics of induction motors. Also, it is mentioned that further work is needed in coming up with a more robust aggregate load model in order to capture future FIDVR-type events.

The authors in [16] present a methodology to model the effects of stalled induction motors. They model air conditioners as standard induction motors in PSS/E in normal running conditions. In order to model stalled air conditioners they scale the nominal power equations with the stalled condition current in order to capture the increased power consumption. They assume fixed values of pre-stall and post-stall power factors and locked-rotor current. They compare the results of this model with the standard PSS/E "CLOD" load model and show that their model reflects the sustained increase in active and reactive power consumption after the motor stalls.

P. Pourbeik and B. Agrawal propose a hybrid model to represent the behavior of air conditioner motors in [17]. In order to demonstrate the air conditioner motor stalling behavior, their model switches from a standard 3-phase induction motor model to a constant impedance model when the motor terminal voltage goes below a certain pre-defined value. They validate this model based on data from an event that occurred on the Arizona Public Services (APS) system in 2003. They also point out that the model is significantly sensitive

to the "stall voltage" of motors (the pre-defined value below which the model switches to constant impedance). A similar approach is used in [18].

The Western Electricity Coordinating Council (WECC) Load Modeling Task Force (LMTF) is in its final stages of developing a detailed composite load model which includes a performance model to capture the stalled behavior of air conditioner motors [19]. In 1997, WECC started using the "interim" load model for its studies. The "interim" load model consisted of 20% load represented by induction motors and 80% load represented by the static ZIP model. Although this model was able to validate against major observed disturbances, it was not able to capture delayed voltage recovery due to air conditioner stalling in the event of a fault. In 2002, the WECC LMTF was formed to come up with a more appropriate composite load model. The present composite load model includes a performance model for air conditioner motors and is considered to be good enough to model these motors and capture FIDVR-type events. The performance model is represented by a static exponential model during normal running conditions whose parameters are decided based on experimental test data and by a constant impedance during the stalled condition. This is found to be good enough to match the observed power and current measurements during various experiments. Although this model doesn't capture the motor dynamics, it has been justified by the fact that since A/C compressor motors have very low inertias (of the order of 0.05 seconds), they switch from the running state to the stalling state within a few cycles and not much information is lost during these few cycles. The model switches from the static exponential model to constant impedance model based on the terminal voltage going below a certain pre-defined value, similar to the approach adopted in [17, 18]. It is

found that this pre-defined voltage value is a function of the ambient temperature and the fault duration. This value typically ranges from 0.5 to 0.6 p.u.

In this thesis, the dynamic A/C motor model presented in [1] is considered. The model accurately captures the dynamics of the machine and also demonstrates the stalled behavior of these machines. The model has been found to be rich enough to model air conditioner loads both during steady-state operation and transients.

The performance model that switches from an exponential static model to a constant impedance model depending on the terminal voltage going below a pre-defined value has to deal with the uncertainty involved in selecting the right pre-defined value for the equivalent model representing the aggregated effect of several machines in an area. If one motor stalls, it draws an excessively high amount of current in its stalled state, leading to a further drop in voltage. This drop in voltage may lead to the stalling of other motors having a slightly lower pre-defined voltage setting, leading to cascaded stalling of motors. In order to capture such a phenomenon, one solution is to set the pre-defined voltage value of the equivalent motor model at the value corresponding to the highest pre-defined value among all the motors in that area. Another approach is to set the value at the weighted average value of all the motors in the area. Both these approaches are not the best approaches to model the aggregate effect of several A/C motors in an area.

The authors in [20] propose an aggregation method for induction motors based on the conventional steady-state performance equations. Their procedure satisfies the power invariance condition, neglects the stator resistance and places the magnetizing reactance at the motor terminals. The motor circuits are then connected in parallel and are reduced to a

single equivalent circuit representing the aggregate motor. To determine the inertia constant of the aggregate motor, they used the KVA weighted average of individual motor inertia constants. Most other recent methods combine several motors into a single equivalent motor at a particular bus such that the power drawn by the equivalent motor equals the net power drawn by the individual motors.

A more refined approach to aggregate air conditioners based on their stalling behavior is presented in this work. Analytical tools based on bifurcation theory are used to characterize different operating scenarios possible for different system conditions.

1.3 Bifurcation Analysis in Power Systems

Electric power systems are large physical systems interconnecting various devices to perform generation, delivery, and consumption of electricity. From an engineering point of view, the task in the power system operation is to maintain proper frequency and voltage magnitude within appropriate tolerance so that the system may operate at a stable equilibrium point in the steady-state. Power system equilibrium equations which determine the system's operating state typically depend on a very large number of parameters. Hence, numerous parameters such as generation, load, network conditions, etc., that can change with time and circumstances affect the system behavior. Under normal variations of those parameters, the operating point varies smoothly and so the variation can be tracked by local linear analysis. However, this behavior changes qualitatively at certain critical parameter values such that the equilibrium point becomes unstable causing operational problems. One such operational problem occurs in the area of system voltage magnitude, which is affected due to various phenomena such as A/C motor stalling. This voltage decrement could be spread

uncontrollably throughout the power system causing a total (blackout) or partial disruption of the power system operation. The phenomenon of this catastrophic event is referred to as a voltage collapse. Voltage collapse problems are considered to be the principal threat to power system stability, security and reliability in many utilities around the world [21]. Several methods have been proposed to find the critical parameters that make an equilibrium point unstable or disappear, producing a voltage collapse [21]. Bifurcation theory has received considerable attention from researchers to increase the understanding of the complex behavior associated with the voltage collapse phenomenon [22, 23, 24].

Bifurcation theory refers to characterizing sudden changes in the qualitative response of the system as its parameters are varied smoothly and continuously over a specified range. When these changes relate to qualitative changes occurring in the neighborhood of an equilibrium point or limit cycle such that an equilibrium point or limit cycle appears, disappears, or loses stability, they are referred to as local bifurcations. In bifurcation problems, it is very useful to consider a space formed by the system state variables and parameters, called the state-control space. In this space, locations at which bifurcations occur are called bifurcation points. The numerical analysis to locate these points is based on the principle of continuation. Several people have proposed different implementations of the continuation method in the literature to detect bifurcations in power systems [25, 26, 27, 28, 29].

A continuation method generates a chain of solutions from an established solution of the equations representing the system under analysis. The solution branch thus established can then be examined for bifurcation points, at which a qualitative change can be observed.

The representation of this branch of solutions in the state-control space is referred to as a bifurcation diagram. The stability properties of the bifurcation diagram can be studied by established analysis techniques such as eigenvalue analysis.

The authors in [30] present the bifurcation analysis of a detailed power system model consisting of an aggregated induction motor load and impedance load. They use detailed differential equation models for the generator system, short transmission system and the loads. The induction motor is modeled using a standard 3-phase dq0 model. The load torque on the motor is modeled as a linear function of the rotor speed and the coefficient that sets the slope of this function is considered as the free parameter in order to perform bifurcation studies. They show that first order induction motor models are adequate for saddle-node bifurcation studies, whereas steady-state models are not adequate for such analyses. Further, they conclude that when oscillatory modes associated with Hopf bifurcation are to be studied, higher order motor models must be used.

The authors in [31] study the effect of induction motor stalling on power system voltage stability using bifurcation theory. The mechanical load torque is modeled as a linear function of a free parameter. A two motor, four bus system is considered for the analysis. The plot of the motor terminal voltage vs the torque parameter is used to study motor cascaded stalling. They show that there is a possibility of cascaded stalling if one of the motors stalls first, depending on the coefficient of the free parameter for each of the two motors.

In this work, a continuation method is used to solve for equilibrium points of a system consisting of two phasor modeled A/C motors connected to a voltage source through a simple

impedance network. While allowing the source voltage to vary freely, the algorithm solves for various steady-state operating points. Eigenvalue analysis is used to arrive at stable regions of operation. This information would prove to be very useful in coming up with a methodology to model the aggregated effect of air conditioner motors in order to appropriately model a large number of such machines in the system.

Chapter 2 Modeling and Simulation

This chapter presents the modeling and simulation approaches adopted in this thesis to model an air conditioner compressor motor. Simulation results of various tests performed on this model are presented. A phasor modeling approach is used to model the air conditioner compressor motor. The Differential Algebraic Impulsive Switched (DAIS) model is used for the simulations and also to obtain trajectory sensitivities to changes in various model parameters. Trajectory sensitivities give a good estimate of the more significant parameters that influence the performance of the model. In the following sections of this chapter, the theoretical models are presented. Next, the results of the simulations are presented.

2.1 Phasor Model of Air Conditioner Compressor Motors

The mathematical model presented in [1] is considered here. It is well known that a typical air conditioner compressor motor consists of a single phase induction motor. The load torque of these machines is typically constant for various speeds of operation. The phasor model accurately captures the dynamics of the machine and also demonstrates the stalled behavior of these machines. The model has been found to be rich enough to model air conditioner loads both during steady-state operation and transients.

The mathematical equations governing the model behavior are as follows [1]:

$$\left|V_s\right| = \left(r_{ds} + j\frac{\omega_s}{\omega_b}X_{ds}'\right)\left(I_{ds}{}^{R} + jI_{ds}{}^{I}\right) + j\left(\frac{\omega_s}{\omega_b}\right)\frac{X_m}{X_r}\left(\Psi_{dr}{}^{R} + j\Psi_{dr}{}^{I}\right) \qquad (2.1)$$

$$\left|V_s\right| = \left(r_{qs} + j\frac{\omega_s}{\omega_b}X_{qs}' + j\frac{\omega_b}{\omega_s}X_c\right)\left(I_{qs}{}^R + jI_{qs}{}^I\right) + j\left(\frac{\omega_s}{\omega_b}\right)\frac{nX_m}{X_r}\left(\Psi_{qr}{}^R + j\Psi_{qr}{}^I\right) \tag{2.2}$$

$$\begin{bmatrix}\left(\Psi_f{}^R + j\Psi_f{}^I\right)\\ \left(\Psi_b{}^R + j\Psi_b{}^I\right)\end{bmatrix} = \frac{1}{2}\begin{bmatrix}1 & -j\\ 1 & j\end{bmatrix}\begin{bmatrix}\left(\Psi_{dr}{}^R + j\Psi_{dr}{}^I\right)\\ \left(\Psi_{qr}{}^R + j\Psi_{qr}{}^I\right)\end{bmatrix} \tag{2.3}$$

$$\begin{bmatrix}\left(\Psi_{dr}{}^R + j\Psi_{dr}{}^I\right)\\ \left(\Psi_{qr}{}^R + j\Psi_{qr}{}^I\right)\end{bmatrix} = \begin{bmatrix}1 & 1\\ j & -j\end{bmatrix}\begin{bmatrix}\left(\Psi_f{}^R + j\Psi_f{}^I\right)\\ \left(\Psi_b{}^R + j\Psi_b{}^I\right)\end{bmatrix} \tag{2.4}$$

$$\begin{bmatrix}\left(I_f{}^R + jI_f{}^I\right)\\ \left(I_b{}^R + jI_b{}^I\right)\end{bmatrix} = \frac{1}{2}\begin{bmatrix}1 & -jn\\ 1 & jn\end{bmatrix}\begin{bmatrix}\left(I_{ds}{}^R + jI_{ds}{}^I\right)\\ \left(I_{qs}{}^R + jI_{qs}{}^I\right)\end{bmatrix} \tag{2.5}$$

$$\begin{bmatrix}\left(I_{ds}{}^R + jI_{ds}{}^I\right)\\ \left(I_{qs}{}^R + jI_{qs}{}^I\right)\end{bmatrix} = \begin{bmatrix}1 & 1\\ j/n & -j/n\end{bmatrix}\begin{bmatrix}\left(I_f{}^R + jI_f{}^I\right)\\ \left(I_b{}^R + jI_b{}^I\right)\end{bmatrix} \tag{2.6}$$

$$T_o'\frac{d}{dt}\left(\Psi_f{}^R + j\Psi_f{}^I\right) = X_m\left(I_f{}^R + jI_f{}^I\right) - \left(sat(\Psi_f, \Psi_b) + j(\omega_s - \omega_r)\,T_o'\right)\left(\Psi_f{}^R + j\Psi_f{}^I\right) \tag{2.7}$$

$$\left(\Psi_b{}^R + j\Psi_b{}^I\right) = \frac{X_m\left(I_b{}^R + jI_b{}^I\right)}{\left(sat(\Psi_f, \Psi_b) + j(\omega_s + \omega_r)\,T_o'\right)} \tag{2.8}$$

$$\frac{2H}{\omega_b}\frac{d\omega_r}{dt} = \frac{X_m}{X_r}2\left(I_f{}^I\,\Psi_f{}^R - I_f{}^R\,\Psi_f{}^I - I_b{}^I\,\Psi_b{}^R + I_b{}^R\,\Psi_b{}^I\right) - T_{mech} \tag{2.9}$$

$$I_s = \left[\left(I_{ds}{}^R + jI_{ds}{}^I\right) + \left(I_{qs}{}^R + jI_{qs}{}^I\right)\right]e^{j\varphi} \tag{2.10}$$

$$sat(\Psi_f\,, \Psi_b) = \begin{cases}1 & \text{for } \Psi \le b_{sat}\\ 1 + A_{sat}\left(\Psi - b_{sat}\right)^2 & \text{for } \Psi \ge b_{sat}\end{cases} \tag{2.11}$$

$$\text{and } \Psi = \sqrt{\left(\Psi_f{}^R\right)^2 + \left(\Psi_f{}^I\right)^2 + \left(\Psi_b{}^R\right)^2 + \left(\Psi_b{}^I\right)^2} \tag{2.12}$$

Where,

V_s – applied voltage phasor,

ω_s – applied voltage frequency,

φ – applied voltage phase angle,

ω_b – frequency base,

H – motor inertia,

n – ratio of stator auxiliary winding turns to stator main winding turns,

T_{mech} – mechanical load torque,

r_{ds} – d-axis stator resistance,

r_{qs} – q-axis rotor resistance,

X_{ds}' – d-axis stator transient reactance,

X_{qs}' – q-axis stator transient reactance,

X_m – magnetizing reactance,

X_r – rotor reactance,

X_c – capacitive reactance,

A_{sat} – saturation constant,

b_{sat} – saturation constant,

T_o' – rotor time constant,

and,

ω_r – motor speed,

I_{ds}^R – real part of d-axis stator current,

I_{ds}^{I} – imaginary part of d-axis stator current,

I_{qs}^{R} – real part of q-axis stator current,

I_{qs}^{I} – imaginary part of q-axis stator current,

Ψ_{dr}^{R} – real part of d-axis rotor flux voltage,

Ψ_{dr}^{I} – imaginary part of d-axis rotor flux voltage,

Ψ_{qr}^{R} – real part of q-axis rotor flux voltage,

Ψ_{qr}^{I} – imaginary part of q-axis rotor flux voltage,

Ψ_{f}^{R} – real part of forward rotating flux voltage,

Ψ_{f}^{I} – imaginary part of forward rotating flux voltage,

Ψ_{b}^{R} – real part of backward rotating flux voltage,

Ψ_{b}^{I} – imaginary part of backward rotating flux voltage,

I_{f}^{R} – real part of forward current,

I_{f}^{I} – imaginary part of forward current,

I_{b}^{R} – real part of backward current,

I_{b}^{I} – imaginary part of backward current,

I_s – stator current,

$sat(\Psi_f , \Psi_b)$ – saturation function.

It can be seen that this model is a 3^{rd} order differential-algebraic model with saturation effects incorporated and it captures the detailed electrical behavior of these

machines. In order to simulate the dynamical behavior of the A/C motors, the phasor model is developed in the DAIS framework, which is briefly described in the following section.

2.2 Differential-Algebraic Impulsive Switched Model

The usual approach to model a power system is using a differential-algebraic set of equations (DAE) of the form:

$$\dot{x} = f(x , y) \tag{2.13}$$

$$0 = g(x , y) \tag{2.14}$$

Where,

$$x \in \mathbf{R}^n$$

$$y \in \mathbf{R}^m$$

$$f : \mathbf{R}^{n+m} \rightarrow \mathbf{R}^n$$

$$g : \mathbf{R}^{n+m} \rightarrow \mathbf{R}^m$$

x is a vector of n dynamic state variables,

y is a vector of m algebraic state variables.

The differential variables (dynamic state variables) typically include the mechanical states of the generators, the electrical states of the generator rotor, the excitation and governor systems (voltage and frequency controls respectively), and the dynamic states of the loads. The algebraic states are mainly determined by the transmission network and algebraic states of the generator stator and the loads. The parameters of the system such as resistances, inductances, capacitances, etc., can be included in the x variables by making sure that corresponding to each parameter p, a trivial differential equation,

$$\dot{p} = 0 \tag{2.15}$$

is included in the f equations. One way to think of the DAE structure is to consider the function g as describing an m-dimensional manifold to which the differential equation set f is constrained. Power systems often involve several switching actions and transformer tap changes. To incorporate such events into a modeling framework, an extension to the DAE structure can be used. This framework has been called the Differential-Algebraic Impulsive Switched (DAIS) model [5, 6]. Symbolically, it can be represented as:

$$\dot{x} = f(x , y) \tag{2.16}$$

$$0 = g(x , y) \tag{2.17}$$

$$0 = g^{-}(x , y) \text{ if } s(x , y) < 0 \tag{2.18}$$

$$0 = g^{+}(x , y) \text{ if } s(x , y) > 0 \tag{2.19}$$

$$x^{+} = h^{-}(x^{-}, y^{-}) \text{ if } s(x , y) = 0 \tag{2.20}$$

Where, s(x , y) represents the switching function that decides which equations are to be considered depending on the status of an event. The DAIS model captures all the important aspects of hybrid system behavior, namely, the interaction between continuous and discrete states as they evolve over time. The time varying solutions to this system of equations are given by the time varying trajectories of the system. Trajectories describe the behavior of the dynamic states x and the algebraic states y over time. More formally, flows of x and y can be defined as:

$$\varphi(x_o , t) = \begin{bmatrix} \varphi_x(x_o , t) \\ \varphi_y(x_o , t) \end{bmatrix} = \begin{bmatrix} x(t) \\ y(t) \end{bmatrix} \tag{2.21}$$

Where,

x_o represents the initial conditions of the model,

$\varphi_x(x_o , t)$ represents the flow of x,

$\varphi_y(x_o , t)$ represents the flow of y,

$\varphi(x_o , t)$ represents the system flow.

To explore the effect of small changes in the parameters and/or initial conditions on the system flow, it is useful to look at the trajectory sensitivities. Trajectory sensitivity analysis provides a way of quantifying the changes in the flow of the system that result from small changes in parameters and/or initial conditions of the states. Rather than linearizing around an operating point, trajectory sensitivities are the linearization around a nominal trajectory. The trajectory sensitivities can be obtained by forming a Taylor series expansion of the flow equations (2.21). The resulting approximate changes in trajectories due to small changes in initial conditions are given by,

$$\Delta x(t) = \frac{\partial x(t)}{\partial x_o} \Delta x_o \equiv \Phi(x_o , t)\, \Delta x_o \qquad (2.22)$$

$$\Delta y(t) = \frac{\partial y(t)}{\partial x_o} \Delta x_o \equiv \Psi(x_o , t)\, \Delta x_o \qquad (2.23)$$

Where,

$\Phi(x_o , t)$ – trajectory sensitivities of x(t),

$\Psi(x_o , t)$ – trajectory sensitivities of y(t).

Details of the computation of trajectory sensitivities over time, both away from events and at events are given in [5]. The solution of the DAIS model at each time step may be obtained by applying the Newton's method. The partial derivative matrix or the Jacobian matrix used

in the Newton's method to find the next point in the simulation is the same matrix used in the computation of the trajectory sensitivities.

2.3 Simulation Results

This section presents the simulation results of the phasor modeled A/C motor using the DAIS model. The data corresponds to that of a 240 V, 3.5 ton air conditioner. The model parameter values used for the simulation studies are taken from [1] and are shown in Table 2.1.

Table 2.1 Model Parameter Values.

ω_s = 377 rad/sec	r_{ds} = 0.0365 p.u.	X_r = 2.33 p.u.
ω_b = 377 rad/sec	r_{qs} = 0.0729 p.u.	X_c = -2.779 p.u.
H = 0.04 sec	X_{ds}' = 0.1033 p.u.	A_{sat} = 5.6
n = 1.22	X_{qs}' = 0.1489 p.u.	b_{sat} = 0.7212
T_{mech} = 1.045 p.u.	X_m = 2.28 p.u.	T_{o}' = 0.1212

First, a ramp voltage input is applied to the terminals of the motor. The voltage is shown in Figure 2.1.

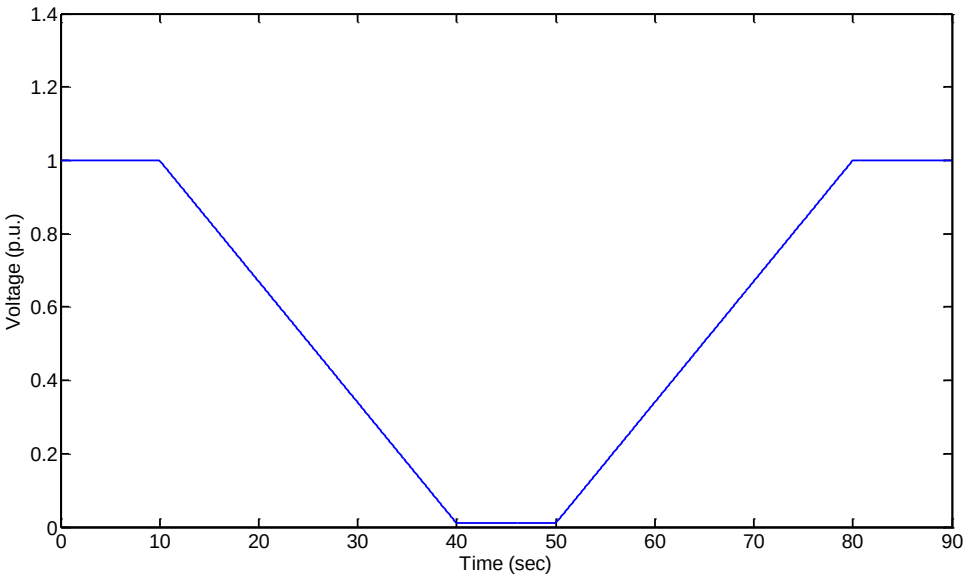

Figure 2.1 Voltage (p.u.) vs Time (sec) for Ramp Test.

The motor starts running with a full voltage of 1 p.u. applied across its terminals. At time = 10 secs, the voltage is ramped down till it reaches a value of 0.01 p.u. at time = 40 secs. In the duration of time = 40 secs to time = 50 secs, the voltage is maintained at this low value. At time = 50 secs, the voltage starts to ramp up until it reaches a value of 1 p.u. at time = 80 secs. Beyond this time, the voltage is maintained at 1 p.u. With this input applied, it is observed that the motor runs at a steady speed until the voltage starts to go down at time = 10 secs. Once the voltage starts ramping down, the motor starts decelerating, as shown in the speed (rad/sec) vs time (sec) plot in Figure 2.2.

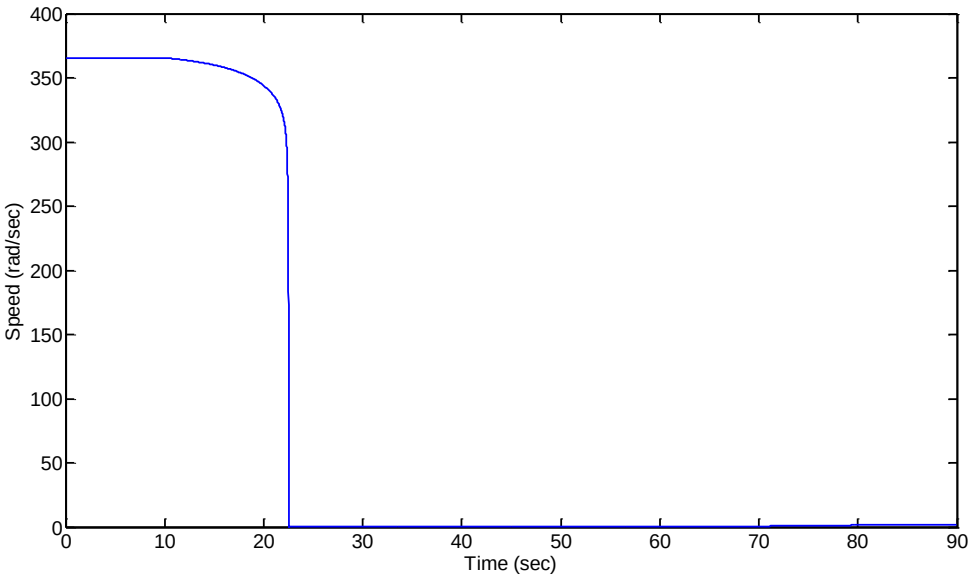

Figure 2.2 Speed (rad/sec) vs Time (sec) for Ramp Test.

At time = 23.5 secs, the motor comes to a complete stop. The terminal voltage at this point is 0.59 p.u. Beyond this point, the motor remains stalled, even when the voltage is ramped up to the nominal 1 p.u. value, as can be seen from Figure 2.2. This accurately captures the stalled behavior of air conditioner motors. The plot of current (p.u.) drawn by the motor vs time (sec) is shown in Figure 2.3. It can be seen that the current drawn by the motor is very high in the stalled condition when the voltage in near its nominal value of 1 p.u. Also, in the stalled condition, the motor current follows the voltage behavior. This is because in the stalled condition, there are no shaft dynamics involved and so, the motor behaves like a constant impedance load whose value corresponds to the locked rotor impedance of the induction motor.

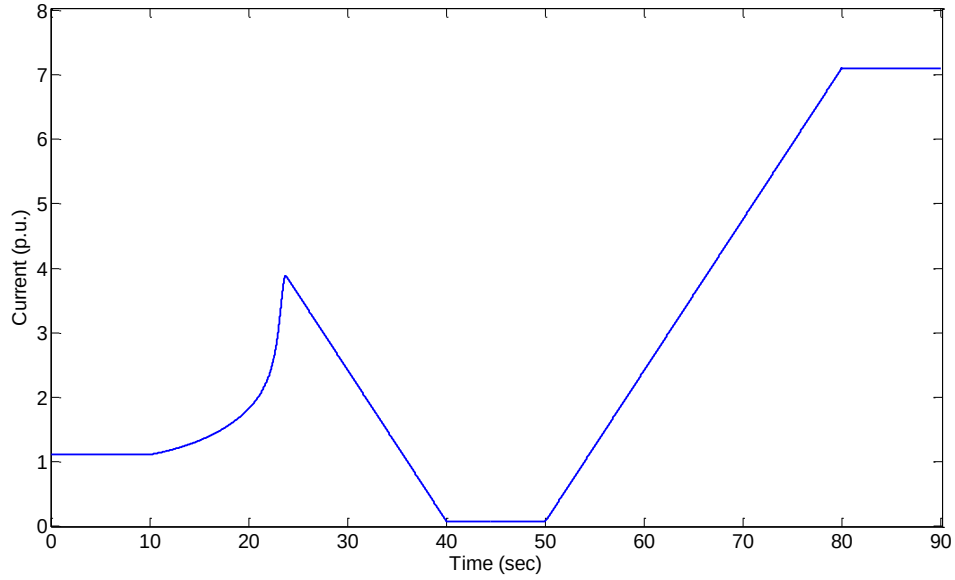

Figure 2.3 Current (p.u.) vs Time (sec) for Ramp Test.

The active and reactive power plots are shown in Figures 2.4 and 2.5 respectively.

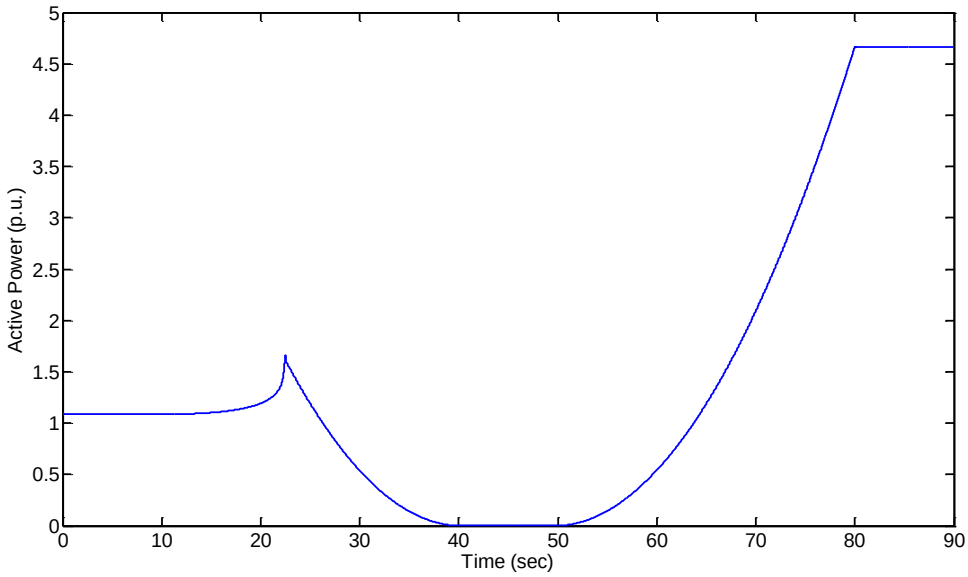

Figure 2.4 Active Power (p.u.) vs Time (sec) for Ramp Test.

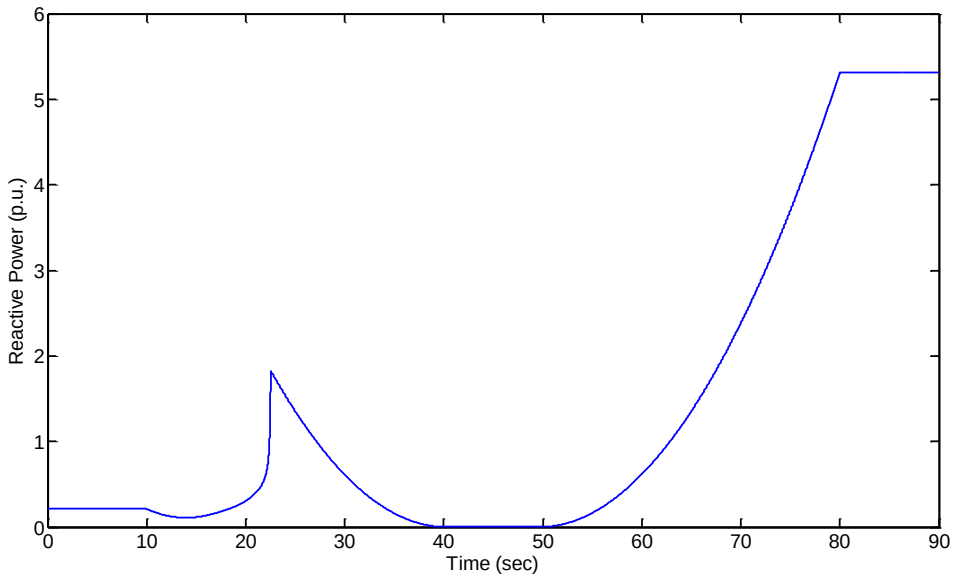

Figure 2.5 Reactive Power (p.u.) vs Time (sec) for Ramp Test.

From these plots it can be seen that the active and reactive power values reach very high values once the motor is in the stalled condition and the voltage reaches near its nominal 1 p.u. value.

Next, the relative importance of the A/C motor model parameters is studied. As mentioned in the previous section, the additional benefit of using the DAIS model is the trajectory sensitivity information. The sensitivity of motor speed, active power and reactive power to various machine parameters is shown in Figures 2.6, 2.7 and 2.8 respectively.

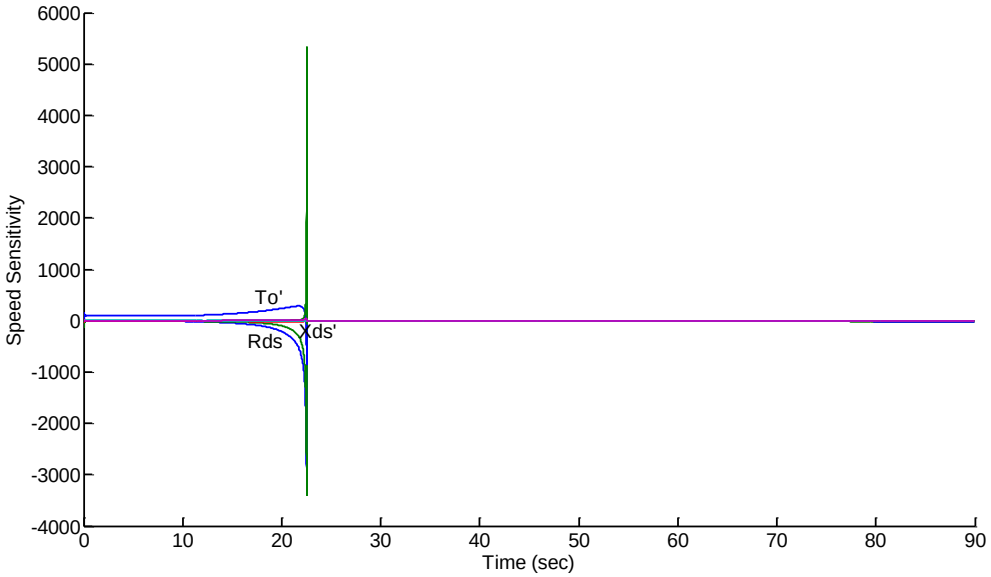

Figure 2.6 Sensitivity of Speed vs Time (sec) for Ramp Test.

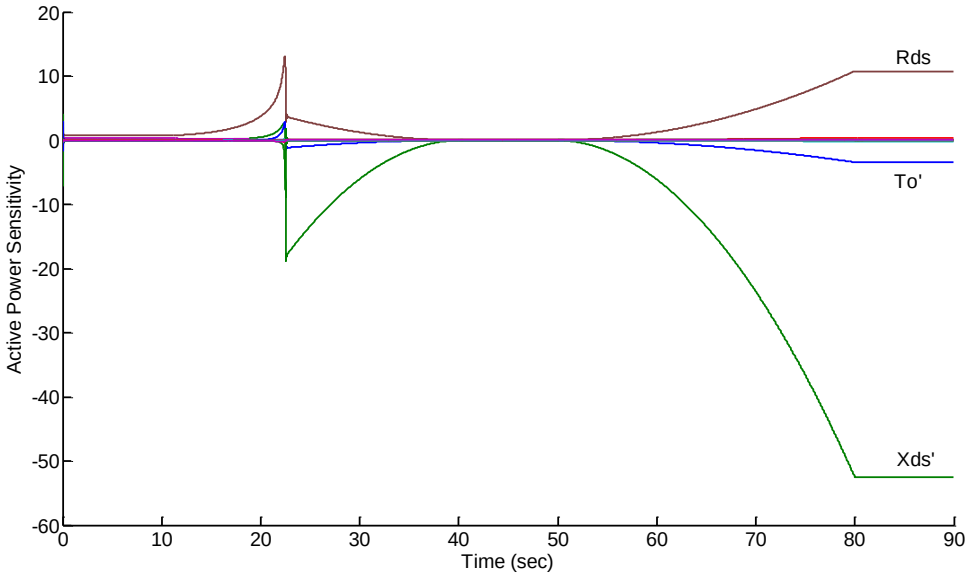

Figure 2.7 Sensitivity of Active Power vs Time (sec) for Ramp Test.

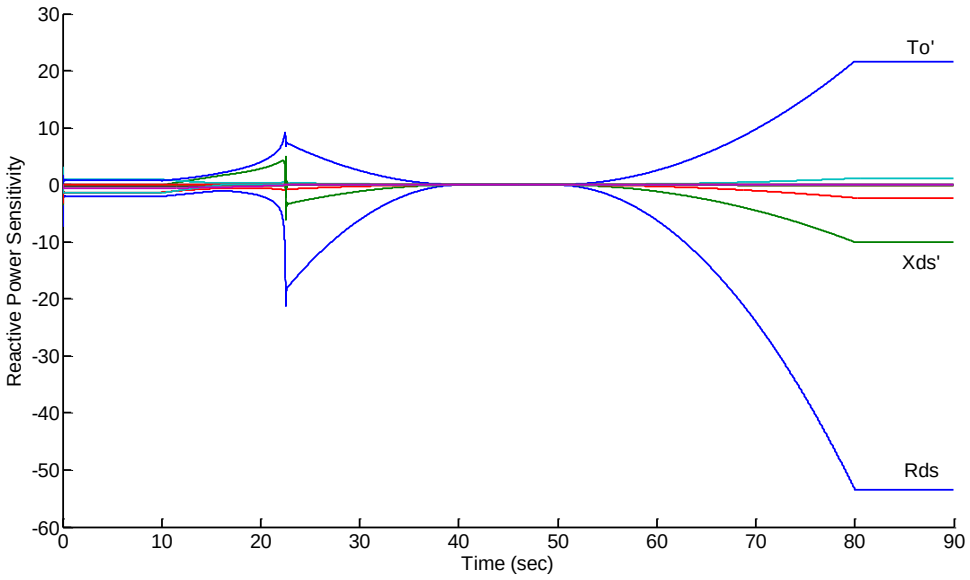

Figure 2.8 Sensitivity of Reactive Power vs Time (sec) for Ramp Test.

Since the machine parameter values are significantly different from each other, a better estimate of the relatively significant parameters may be obtained by looking at the relative sensitivities. That is, by looking at the change in trajectory to a small per unit change in each parameter, while considering the nominal parameter values as the base. This way, one can arrive at an estimate of which parameters are relatively more important than the others. The relative sensitivity of reactive power to various parameters is shown in Figure 2.9.

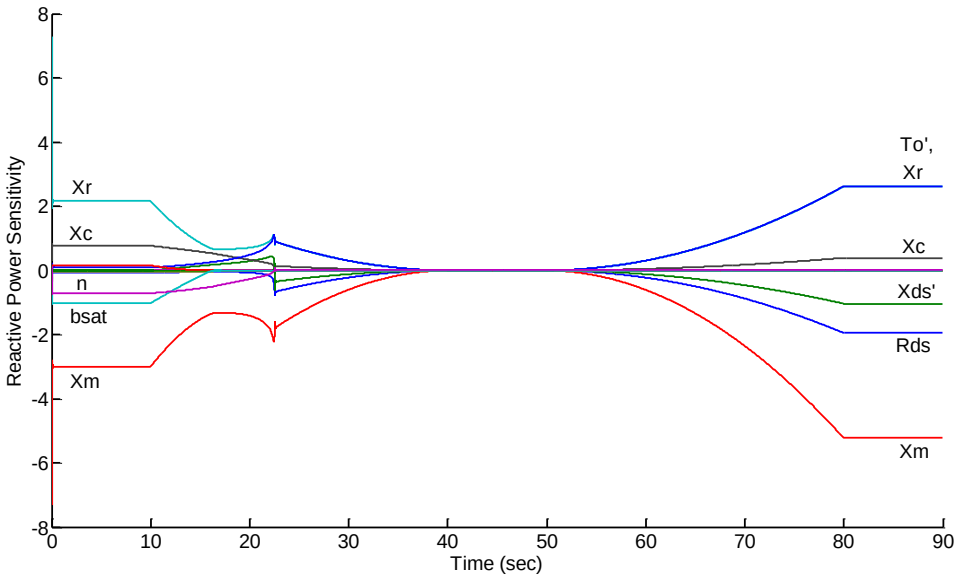

Figure 2.9 Relative Sensitivity of Reactive Power vs Time (sec) for Ramp Test.

From Figure 2.9 it can be seen that in the pre-stall condition, i.e, for time < 23.5 secs, the more sensitive parameters in descending order of sensitivity are X_m , X_r , b_{sat} , X_c and n. In the post-stall condition, i.e, for time > 23.5 secs, the more sensitive parameters in descending order of sensitivity are X_m , X_r , T_o' , r_{ds} , X_{ds}' and X_c . Note that in the post-stall condition, the more sensitive parameters are the stator equivalent circuit resistance and reactance parameters, since in this condition the motor behaves like a constant impedance load.

Next, a sinusoidal voltage is applied across the motor terminals as shown in Figure 2.10.

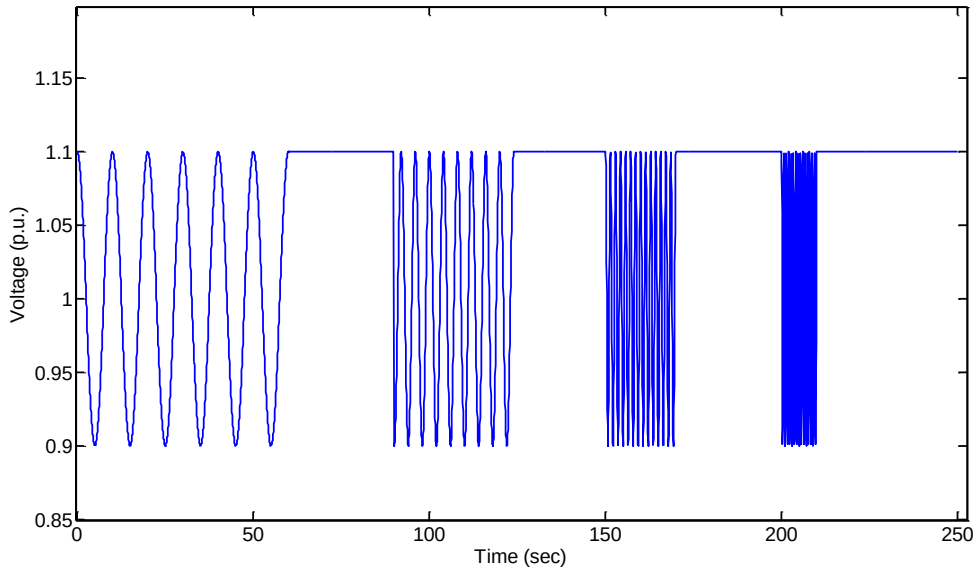

Figure 2.10 Voltage (p.u.) vs Time (sec) for Sinusoidal Test.

The frequency of the voltage is varied every few seconds. Four different frequencies with values 0.1 Hz, 0.25 Hz, 0.7 Hz and 1.5 Hz respectively are considered, as shown in Figure 2.10. The corresponding relative sensitivity of reactive power to various motor parameters is shown in Figure 2.11.

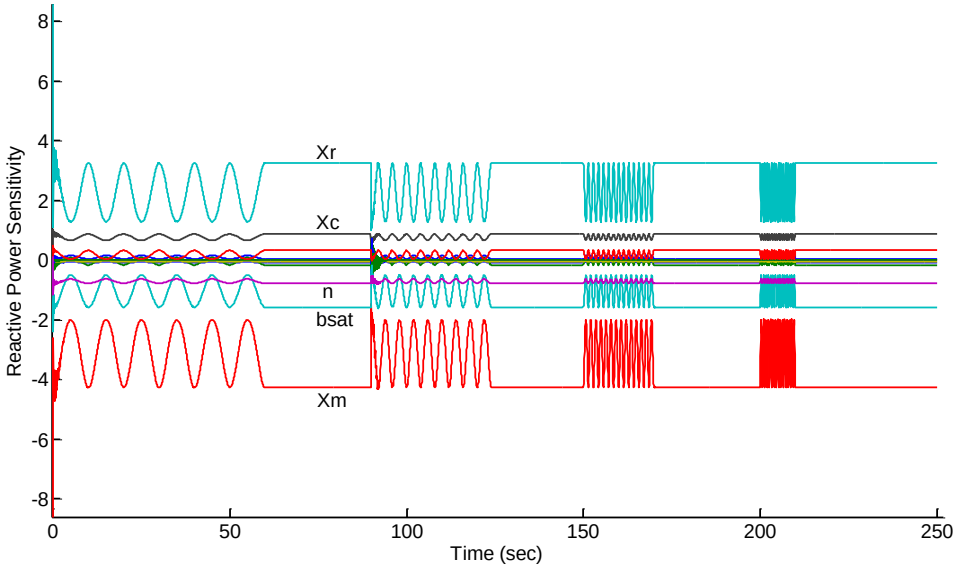

Figure 2.11 Relative Sensitivity of Reactive Power vs Time (sec) for Sinusoidal Test.

From Figure 2.11 it can be seen that the more sensitive parameters are X_m , X_r , b_{sat} , X_c and n, the same as those observed for the ramp voltage test in the pre-stall condition. This information can be effectively used in model parameter validation studies using actual test data. This information of relatively important parameters gives a direction in which the model parameters may be tuned to better estimate all the model parameters.

Chapter 3 Cascaded Stalling

3.1 Background

As mentioned in the introduction, the other challenge in modeling the behavior of A/C compressor motors in power systems is accurate aggregate modeling of these machines. The modeling approaches that use a pre-defined voltage to switch between a normal induction motor model and the constant impedance model to distinguish between a normally running A/C motor and a stalled one use a simplified approach to aggregation. They assume that the motors in a particular area would behave in a similar manner, and hence, aggregate all such motors into a single motor model with a pre-defined stall voltage. It is possible that once an A/C motor stalls in the event of a fault, it results in cascaded stalling of other motors in the system due to the reduction in voltage. It is also possible that stalling of one motor may not lead to the stalling of another. So, it may not be accurate to model the aggregate effect of all the motors in an area by representing them by a single motor. This chapter presents an analytical approach to studying the behavior of several A/C motors in an area during the event of a fault, so that a more accurate methodology to model the aggregate effect of such motors can be adopted.

The approach is based on finding steady-state solutions to a system consisting of more than one A/C motor connected to a source through a network. By allowing the source voltage to vary freely, various operating points of the system can be obtained and the stalling behavior of these motors can be studied. A continuation method based on the predictor-corrector approach is adopted to obtain the steady-state solutions while allowing the source

voltage to be a free parameter. For every value of the source voltage, the system equilibrium point can be obtained by solving for the steady-state conditions. The equilibrium points may undergo a change in their stability properties for certain critical values of the free parameter. To study the qualitative changes in the equilibrium points as the free parameter varies, bifurcation analysis is used.

Bifurcation theory yields tools that are able to classify, study, and give qualitative and quantitative information about the behavior of a non-linear system close to bifurcation or critical equilibrium points as the system parameters change. The parameters are assumed to change slowly, so that the system can be assumed to move from one equilibrium point to another as the parameters change. Hence, bifurcation analysis is usually associated with the study of equilibria of non-linear system models [32]. One type of bifurcation that is commonly observed in power system models is the saddle-node bifurcation (SNB). Saddle-node bifurcations are characterized by two equilibrium points, typically one stable (s.e.p.) and one unstable (u.e.p.), merging at the bifurcation point for a particular parameter value. This equilibrium point has a simple and unique zero eigenvalue of the Jacobian of the linearized system. Beyond this point, there is a loss of equilibrium point. The predictor-corrector approach that is used to arrive at the equilibrium points as the free parameter is varied is described in the next section.

3.2 The Predictor-Corrector Approach

The DAIS set of equations for the system as presented in equations 2.13 and 2.14 can be written more compactly as,

$$F(z) = \begin{bmatrix} f(x , y) \\ g(x , y) \end{bmatrix} \tag{3.1}$$

Where,

$$z = \begin{bmatrix} x \\ y \end{bmatrix} \tag{3.2}$$

The aim of a continuation method is to find solutions to F(z) = 0 for various values of a parameter so that resulting changes in the qualitative behavior of the system can be studied. The predictor-corrector approach is adopted to find these solutions [33]. This algorithm is an automated way of finding solutions to F(z) = 0 for various values of a free parameter. The first step in the algorithm, the predictor step, is a way of predicting the next point on the curve. Assume the algorithm starts at a point z_1 which is obtained by solving for the steady-state equations for a particular starting value of the free parameter. The prediction of the next point is obtained by determining the unit vector tangent to the curve at z_1, and moving along that direction at a pre-defined distance k. This k is a scalar control parameter that determines the distance between successive points along the curve. In regions of high curvature, k may need to be small. When the curve is fairly linear, a large value of k would suffice. The unit vector η which is tangential to the curve at z_1 is given by,

$$DF(z_1)\eta = 0 \tag{3.3}$$

$$\|\eta\|_2 = 1 \tag{3.4}$$

Where, $DF(z_1)$ is the Jacobian of F(z) at z_1.

η can be obtained from the QR factorization,

$$DF^T = QR \tag{3.5}$$

Where, Q is orthogonal and R is upper triangular.

The last column of Q is exactly the desired η.

The prediction of the next point is then given by,

$$z_p = z_1 + k\eta \tag{3.6}$$

The next step in the algorithm is to correct to a point z_2 on the curve. This step is called the corrector step. This point is found by solving for the intersection of the curve and a hyperplane which passes through z_p and that is orthogonal to η. The equation of this hyperplane is given by,

$$(z - z_p)^T \eta = 0 \tag{3.7}$$

The point of intersection of the curve and the hyperplane is given by,

$$F^{cont}(z) = \begin{bmatrix} F(z) \\ (z - z_p)^T \eta \end{bmatrix} = 0 \tag{3.8}$$

These set of equations can be solved for to obtain z_2 using a standard Newton's method, where, the Jacobian is given by,

$$DF^{cont} = \begin{bmatrix} DF \\ \eta^T \end{bmatrix} \tag{3.9}$$

This way, the algorithm can be continued to find various points along the curve for different values of a parameter.

3.3 System Description

In order to investigate cascaded stalling of air conditioner motors, a test system as shown in Figure 3.1 is considered. In this system, two motors, M_1 and M_2 with the same ratings as considered in chapter 2 but slightly different electrical parameters are connected to a common bus. These motors are fed by a constant voltage source through a network whose

impedance, Z = (R + jX), is such that at nominal conditions, the voltage drop between the source and the motor terminals is about 4 %. The motors are modeled according to the dynamic phasor model as described in chapter 2. Now, the continuation algorithm as described in the previous section is used to find various solutions for the system operation with the source voltage, V_s, being the free parameter. The idea behind allowing V_s to vary freely is that, in the event of a fault, if one of the two motors stalls, that motor would draw a large amount of current in a stalled condition, which would lead to the motor terminal voltage to drop further. This drop in voltage may lead to the stalling of the second motor. This would not be captured by allowing the motor terminal voltage itself to be a free parameter, since, the effect of stalling of one motor on the terminal voltage would not be reflected in that case. If V_t is the motor terminal voltage, I_s is the current fed by the source to the load bus, I_1 and I_2 are the currents drawn by the two motors respectively, then,

$$V_s = V_t + I_s Z \tag{3.10}$$

$$I_s = I_1 + I_2 \tag{3.11}$$

So, if one motor stalls, it draws a high amount of current, leading to an increase in I_s, in turn leading to a decrease in V_t. This reduction in V_t may lead to stalling of the other motor.

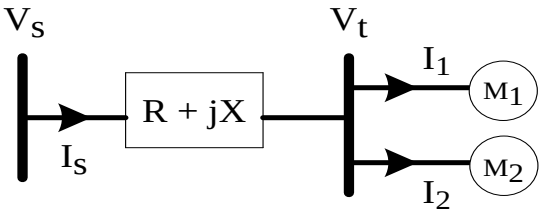

Figure 3.1 Single Line Diagram.

3.4 Results

It is useful to first understand the behavior of a single machine connected to the source through a network, while allowing the source voltage to vary freely. The phasor modeled A/C motor is connected to the source through a network so that the nominal voltage drop between the source and the motor terminals is 4 %.

Figure 3.2 shows the torque-speed curve of the phasor modeled A/C motor. This is obtained by allowing the motor load torque to be the free parameter in the continuation algorithm, while operating at a fixed source voltage of 1 p.u. The green-colored dotted line represents the constant nominal load torque of 1.045 p.u. This plot is very similar to the torque-speed curve of a standard 3-phase induction motor. It is clear from the figure that for a constant torque operation, there exist two operating points for a given value of terminal voltage. The region to the right of the maximum torque point is the stable operating region, while the region to the left of it is the unstable operating region. Different types of load torque characteristics exist depending on the type of the application. The load torque of a fan is typically a quadratic function of the speed of the motor. The load torque of the A/C compressor motors is constant, independent of the speed of the motor. This is the reason why these motors remain stalled once they come to a stop, as the starting torque required to restart these motors at their nominal terminal voltage is not sufficient to meet the constant load torque.

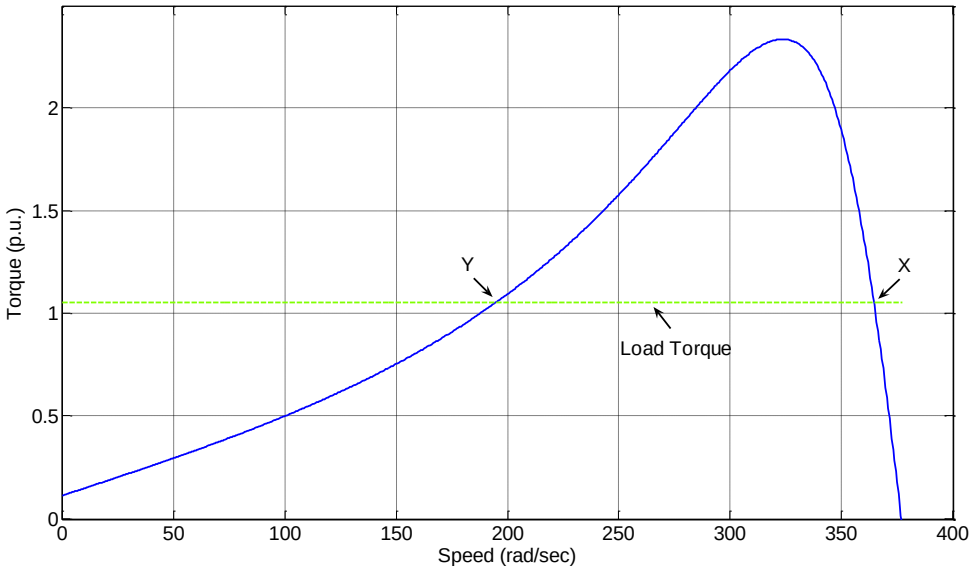

Figure 3.2 Torque (p.u.) - Speed (rad/sec) Curve.

The torque developed by the motor is a function of the terminal voltage. There exists a critical terminal voltage where the maximum torque matches with the load torque. If the voltage is further reduced from this point, the motor would stall. This is shown in Figure 3.3. From Figure 3.3, it can be seen that as the voltage is decreased, the maximum torque decreases, but the speed at which the maximum torque occurs remains the same. This is similar to the behavior of a 3-phase induction motor. The curve marked 'B' represents the plot obtained by operating at a source voltage of 1 p.u. The curve marked 'A' is obtained by operating at a lower voltage. For this curve 'A', the maximum torque matches with the load torque. If the voltage is further reduced from this point, then the motor would stall. Once the motor stalls, it can be seen that the starting torque (torque at speed = 0), also known as the

locked-rotor torque, is smaller than the load torque for all of the curves and so, it remains stalled and cannot restart for any of these voltage values.

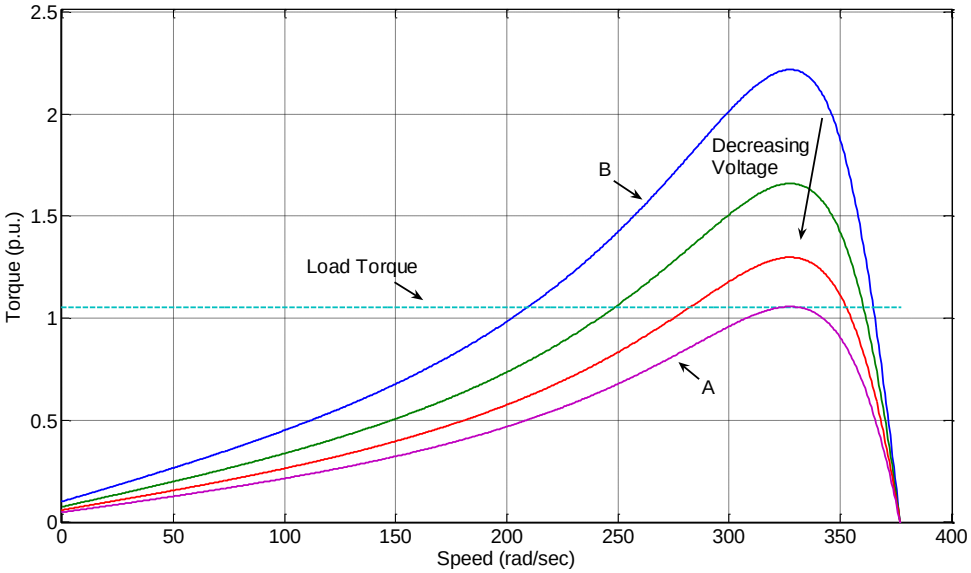

Figure 3.3 Torque (p.u.) - Speed (rad/sec) Curve for Decreasing Voltages.

Figure 3.4 shows various torque-speed curves for various increasing voltages above the nominal voltage. The curve marked 'B' represents the nominal curve where the source voltage is at 1 p.u. The curve marked 'A' represents a curve where the starting torque equals the load torque. If the voltage is further increased from this point, then the starting torque would be greater than the load torque, implying that the motor would be able to restart from the stalled condition. Thus, there exists a critical voltage value below which the motor stalls and remains stalled until a very high voltage is applied across its terminals to overcome the load torque and restart.

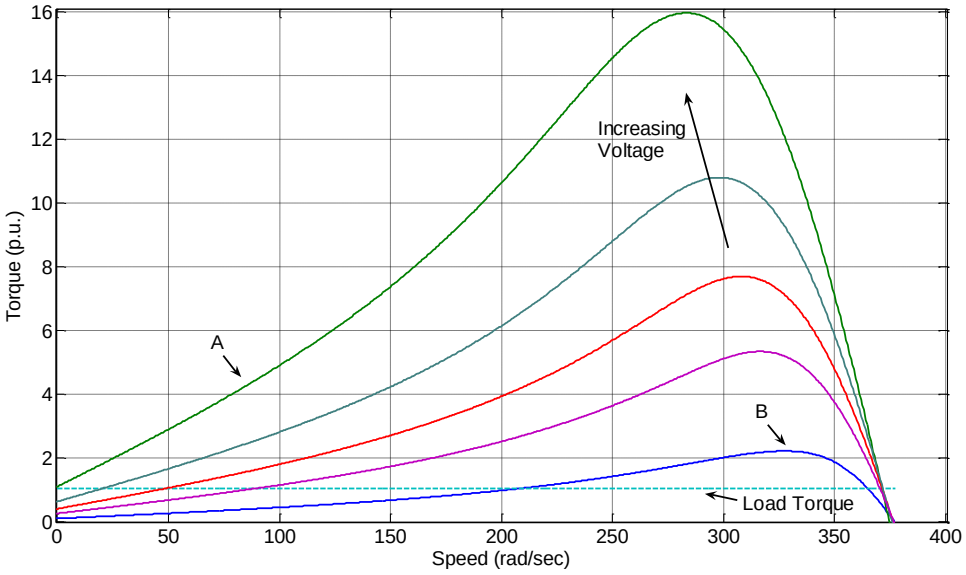

Figure 3.4 Torque (p.u.) - Speed (rad/sec) Curve for Increasing Voltages.

As an aside, it can be seen from Figure 3.4 that the speed at which maximum torque occurs on the torque-speed curve shifts towards the left as the voltage is increased beyond the nominal voltage. This is not seen in Figure 3.3, where the machine is operated at voltages below the nominal voltage. This can be attributed to machine saturation and can be reasoned as follows.

Figure 3.5 shows a plot of the saturation function, sat, as defined in equation 2.11 in chapter 2, vs the motor speed, for various voltages above the nominal voltage. The saturation function is equal to 1 if the machine is not saturated, and is equal to a non-linear function of flux if the machine is saturated, as governed by equation 2.11. From Figure 3.5, it can be seen that as the voltage is increased, the machine is saturated for a wider region of operating speeds. Also, the level of saturation increases as the voltage increases. When the machine

gets saturated, the torque per ampere capability of the machine goes down. More amount of current is required to produce the same amount of torque as compared to the case when the machine is not saturated. To be able to provide a higher amount of current, the machine runs at a lower speed (higher slip) so that the rotor equivalent resistance is lower and in turn the current is higher. Hence, there is a shift in the point where the maximum slip occurs on the torque-speed curve when the machine is operated at higher voltages beyond the nominal voltage.

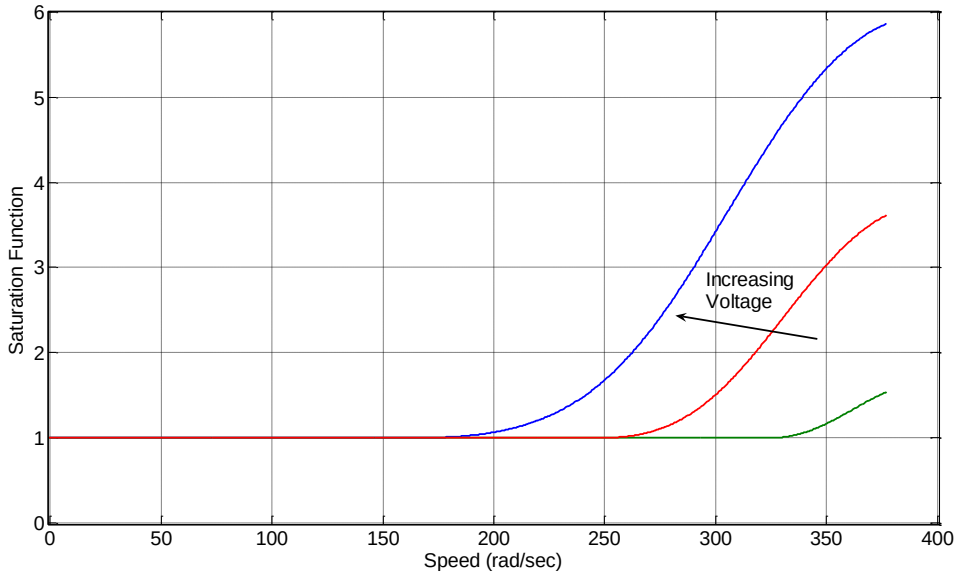

Figure 3.5 Saturation vs Speed (rad/sec).

Now, if the source voltage is considered as the free parameter and the load torque is kept fixed at 1.045 p.u., the operation of the motor for various voltage levels at the source can be studied. Figure 3.6 shows the plot of motor slip vs source voltage (p.u.). In this figure, there are three regions of operation: A-B, B-C, and C-D. The eigenvalue analysis

along these regions shows that the regions A-B and C-D are stable, but the region B-C is unstable. B and C are the saddle-node bifurcation points. B corresponds to the point where the critical source voltage exists such that below that voltage, the motor would stall. In the region A-B, the motor is running normally at various source voltages. When the point B is reached, there is a saddle-node bifurcation. If the voltage is further reduced from this point, the motor enters the stall mode and the operating region corresponds to C-D. In the region C-D, the motor remains stalled even if the voltage is increased from D towards C, until the point C is reached. If the voltage is increased further from C, then the motor starts, since at this voltage it is able to produce sufficient torque to overcome the load torque. Beyond this point, the region of operation is again A-B. Thus, all the regions of operation are captured in this bifurcation diagram.

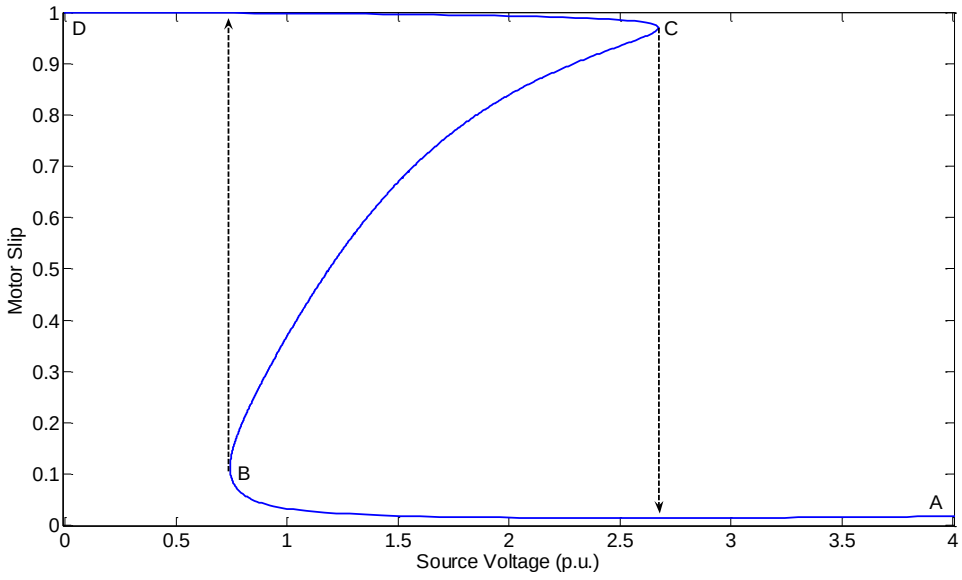

Figure 3.6 Motor Slip vs Source Voltage (p.u.).

For the same system, the plot of the motor terminal voltage (p.u.) vs the source voltage (p.u.) is shown in Figure 3.7. The regions A-B, B-C, and C-D correspond to the ones shown in Figure 3.6. The terminal voltage at point B is found to be 0.6 p.u. Below this critical voltage value, the motor stalls. The terminal voltage at point C is found to be 1.63 p.u. Above this critical voltage value, the motor is able to produce sufficient torque to restart from a stalled condition.

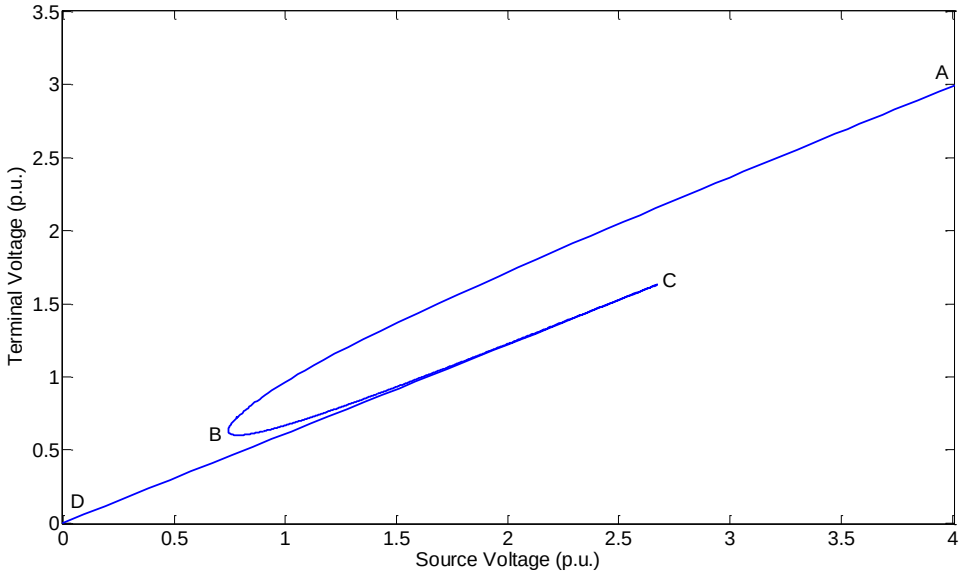

Figure 3.7 Motor Terminal Voltage (p.u.) vs Source Voltage (p.u.).

In order to investigate cascaded stalling of A/C motors, the system shown in Figure 3.1 is considered. For this system, the source voltage is allowed to vary as a free parameter and the continuation algorithm is applied. If the initial conditions of the system are such that both the motors are running at a low slip, the resulting bifurcation diagram shows three possible modes of operation of the two motors. The bifurcation diagram showing the plot of

motor slip vs source voltage (p.u.) for each of the two motors is shown in Figures 3.8 and 3.9 respectively.

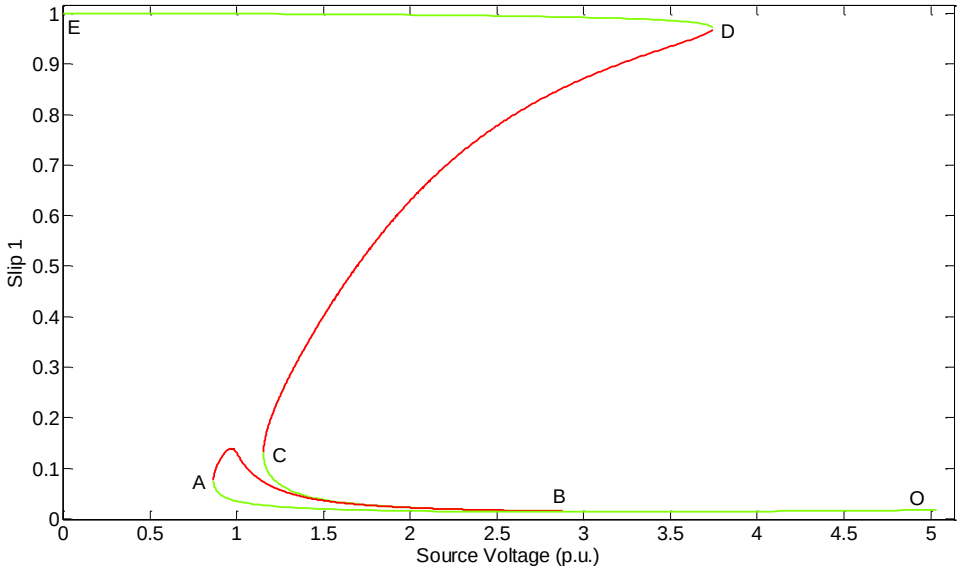

Figure 3.8 Motor 1 Slip vs Source Voltage (p.u.).

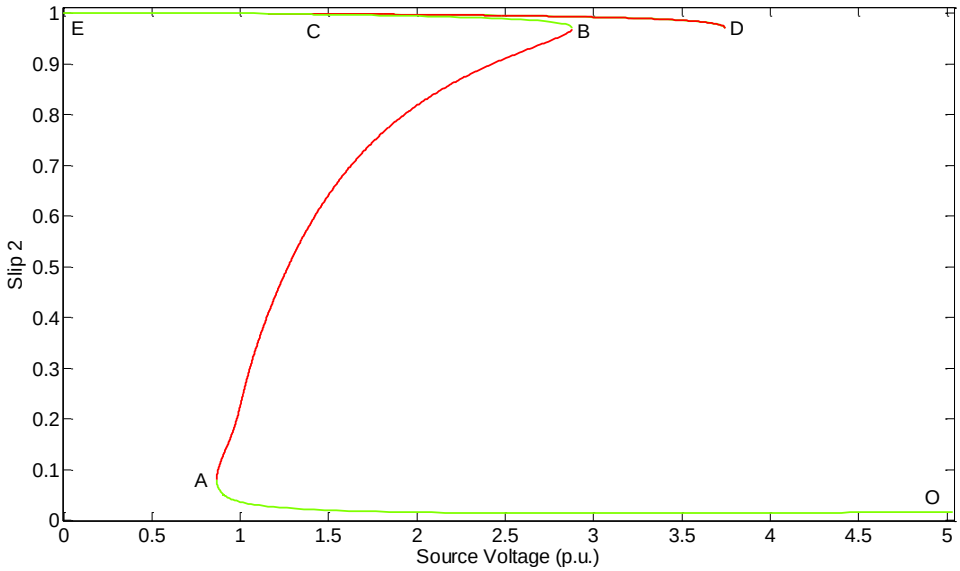

Figure 3.9 Motor 2 Slip vs Source Voltage (p.u.).

The regions of operation of the motors are marked in green and red. Green represents stable region while red represents unstable region. If the initial operating point is the point O in Figures 3.8 and 3.9, both the motors are operating at a low slip (high speed). If the source voltage is consistently decreased from here, both the motors consistently decelerate. Eventually point A is reached beyond which if the source voltage is further reduced, both the motors stall (cascaded stalling) and operate in region D-E in the stalled condition. Suppose, instead of decreasing the voltage at that critical point A the voltage is increased. Then, motor 1 continues operating at a low slip while motor 2 operates closer to stall (region B-C). Beyond point C, if the voltage is further decreased, motor 1 also stalls (cascaded stalling) and the region of operation becomes D-E. Suppose beyond point B, if the voltage is further increased, then motor 1 continues running while motor 2 remains stalled until point D is reached. Beyond the point D, if the voltage is increased, then both the motors run since the torque produced by motor 2 in the stalled condition is sufficient to overcome the load torque and start running. Thus, the stable regions of operation O-A, B-C, and D-E represent three modes of operation of the motors: both running, motor 1 running and motor 2 stalled, and both stalled respectively.

The plot of motor terminal voltage (p.u.) vs the source voltage (p.u.) is shown in Figure 3.10. The regions O-A, A-B, B-C, C-D, and D-E correspond to the same regions of Figures 3.8 and 3.9. At point A, the terminal voltage is around 0.63 p.u. and if the source voltage is slightly reduced from here, then motor 2 stalls. This further decreases the terminal voltage, leading to the stalling of motor 1. Hence, stalling of motor 2 in this case leads to the stalling of motor 1. At point C in Figure 3.10, the terminal voltage is around 0.61 p.u., the

source voltage is 1.15 p.u and motor 2 is stalled. Beyond this point, if the source voltage is further decreased, both the motors are stalled. In the region B-C, only motor 2 is stalled while motor 1 keeps running. So, it is possible to have one motor running while the other is stalled even when both the motors are very similar to each other.

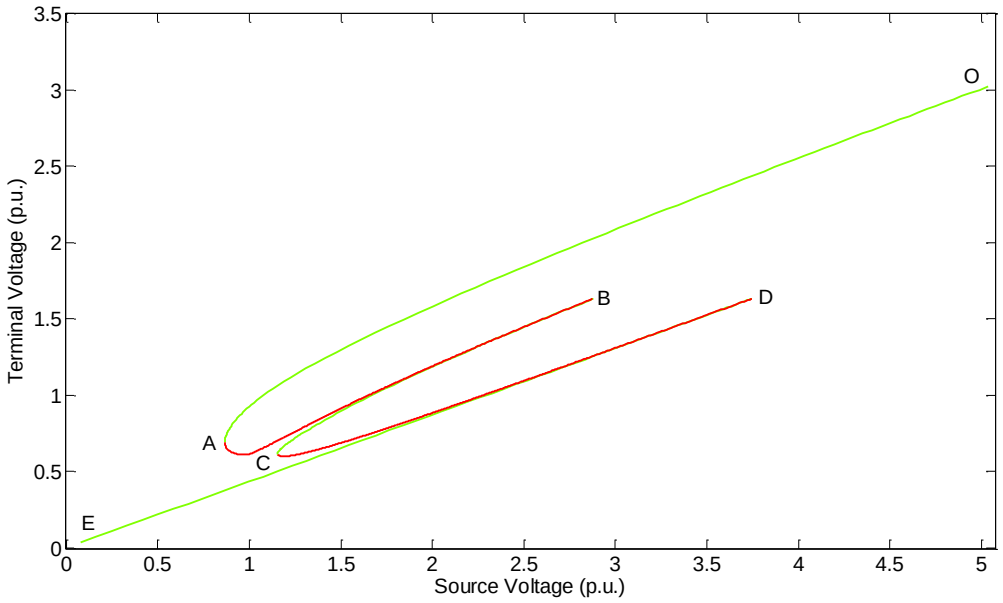

Figure 3.10 Motor Terminal Voltage (p.u.) vs Source Voltage (p.u.).

In order to demonstrate the other mode of operation – motor 1 stalled and motor 2 running, it is useful to start at an initial condition such that motor 1 is running at a high slip (low speed) and motor 2 is running at a low slip (high speed). The resulting bifurcation diagrams are shown in Figures 3.11 and 3.12. The stable regions of operation are O-A, B-C and D-E. O-A represents the region where both the motors are running. B-C represents the region where motor 1 is stalled while motor 2 is running. D-E represents the region where

both the motors are running. Here again, there is a possibility of cascaded motor stalling. There is also a possibility of one motor running while the other one is stalled.

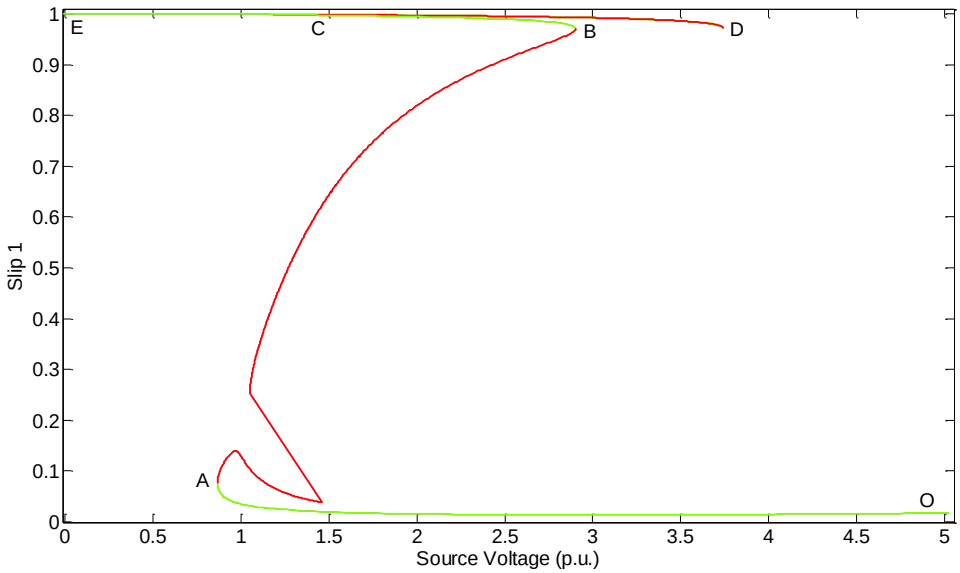

Figure 3.11 Motor 1 Slip vs Source Voltage (p.u.).

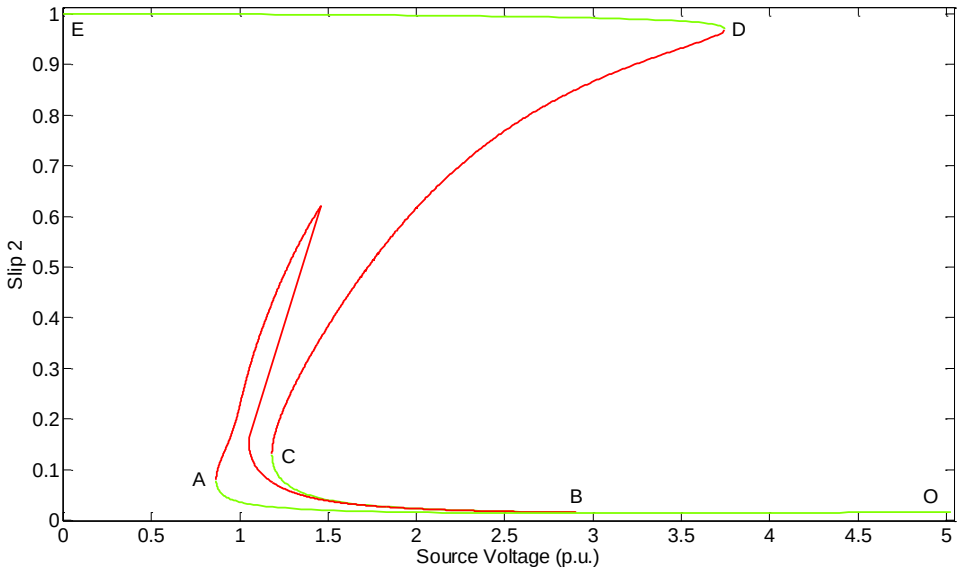

Figure 3.12 Motor 2 Slip vs Source Voltage (p.u.).

Comparing Figures 3.8 and 3.11, it can be seen that the region O-A matches for both these plots. In region A-B, motor 1 either runs at low slip or at high slip and beyond B, motor 1 is either running or stalled. Similarly for motor 2. The high slip region of A-B in Figure 3.11 almost matches with the high slip region A-B of Figure 3.9, indicating that in this case, when initially motor 1 is running at a high slip, its behavior is similar to that of motor 2 in the earlier case where motor 2 was running at high slip. The slight difference in the curves is due to the fact that the two motors do not have identical model parameters. Similar observations can be made for motor 2 by comparing Figures 3.12 and 3.8. From Figure 3.12 it can be seen that at point A, if the voltage is further increased, the motor keeps running at high slip and then, beyond a point jumps to a low slip region instead of continuing towards a stalled condition as seen in Figure 3.9. This low slip region of motor 2 matches closely with the low slip region of motor 1 in the earlier case indicating that its behavior in this case is similar to that of motor 1 in the earlier case.

Thus, depending on the initial operating condition, various modes of operation of the two motors can be observed. This is verified through a dynamic simulation as follows. The same system is considered with both the motors running initially with the source voltage at 1.5 p.u. A fault is created at time = 10 secs such that the motor terminal voltage reaches a value of 0.6 p.u. and stays at that value for a duration of 5 electrical cycles. The voltage comes back to its normal value after the fault is cleared. The corresponding plot of source voltage (p.u.) vs time (sec) is shown in Figure 3.13.

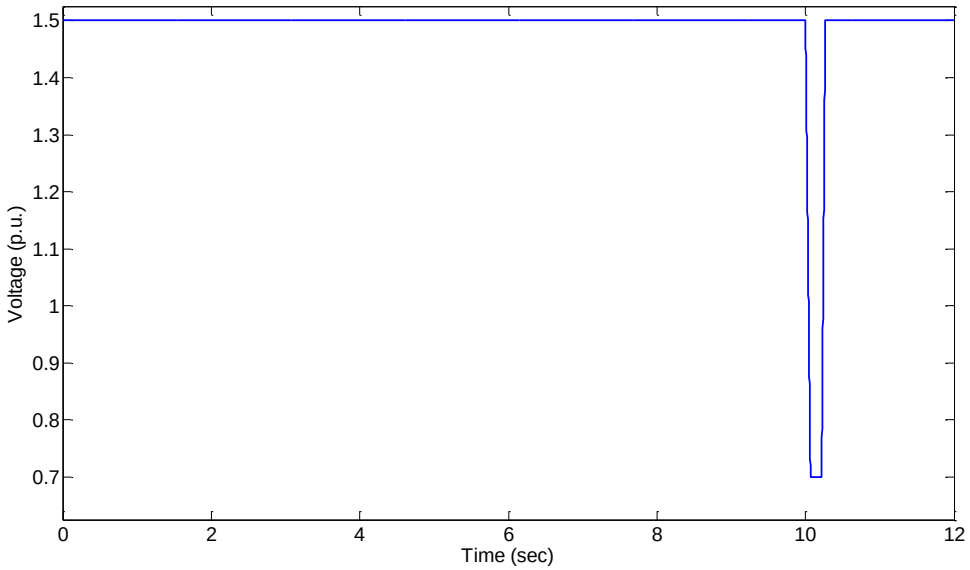

Figure 3.13 Source voltage (p.u.) vs time (sec).

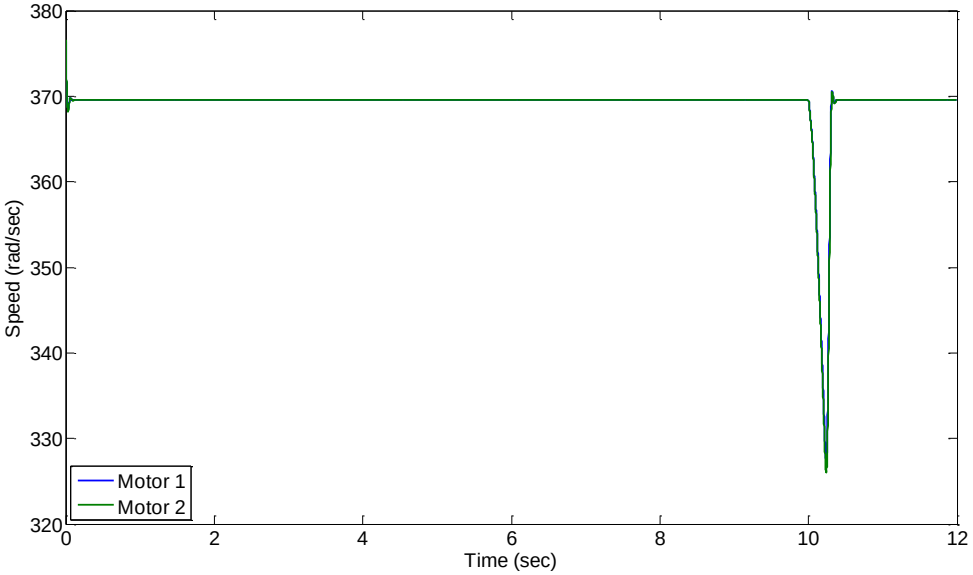

Figure 3.14 Motor Speed (rad/sec) vs time (sec) with both running.

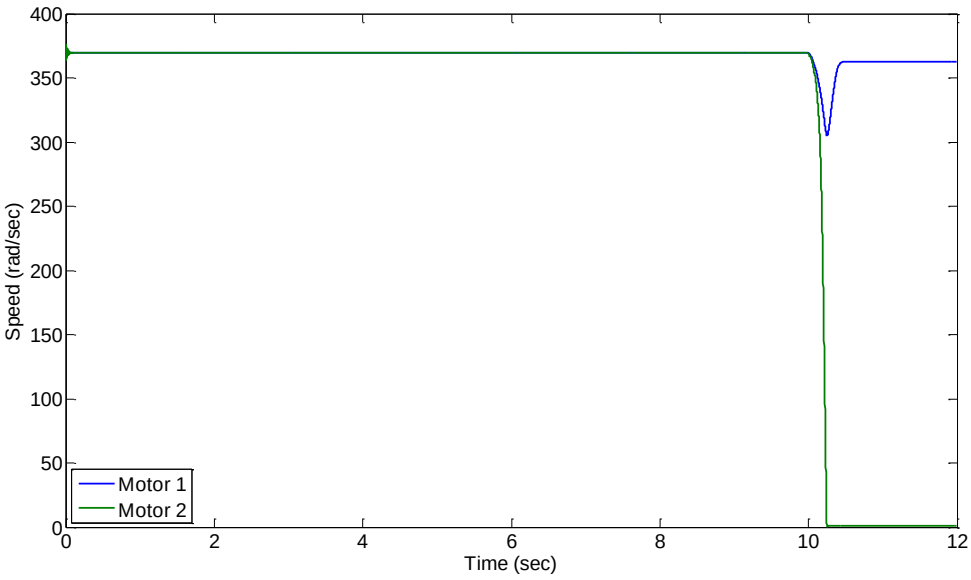

Figure 3.15 Motor Speed (rad/sec) vs time (sec) with one stalled, one running.

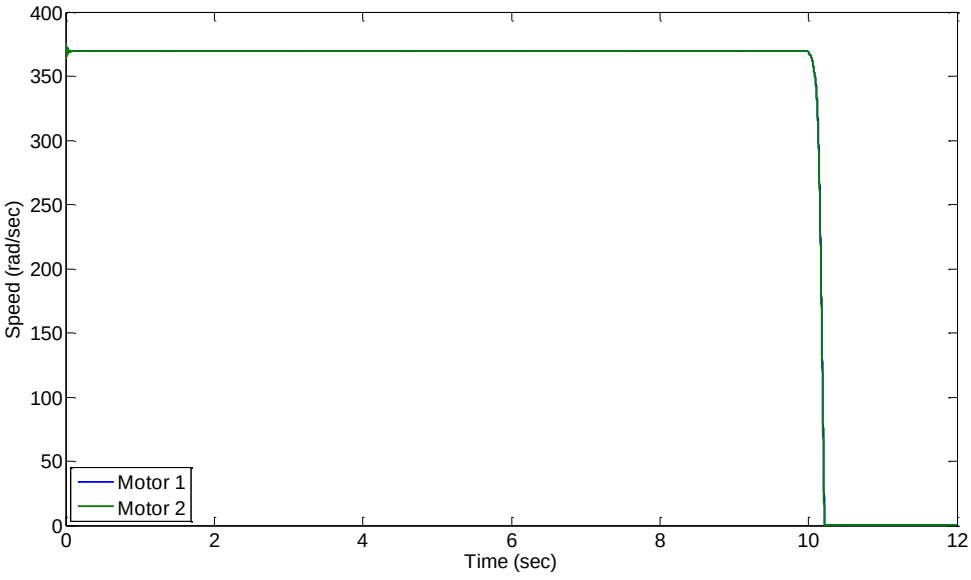

Figure 3.16 Motor Speed (rad/sec) vs time (sec) with both stalled.

Now, for such a voltage input, various modes of operation of the two motors can be obtained by considering motors of various inertias. The steady-state solutions obtained using the continuation algorithm do not get affected by the motor inertias. If both the motor inertias are 0.25 secs each, then the resulting plot of motor speed (rad/sec) vs time (sec) for the motors is as shown in Figure 3.14. The motors decelerate due to a reduction in voltage at time = 10 secs, but regain speed once the voltage comes back to its nominal value. Due to their high inertia, the motors do not come to a stall. Next, for the same system, if the inertia of motor 2 is 0.04 secs, while the inertia of motor 1 is 0.25 secs, then motor 2 stalls but motor 1 keeps running during the same fault, as shown in Figure 3.15. If both the motors have low inertia of 0.04 secs respectively, then both the motors stall as a result of the reduction in voltage. This can be seen in Figure 3.16. If the inertia of motor 1 is 0.04 secs and that of motor 2 is 0.25 secs, then motor 1 would stall while motor 2 would keep running during and after the fault. Thus all the modes of operation are observed when the motors are operating at a source voltage of 1.5 p.u. and a fault occurs at the source terminals.

This indicates that when arriving at an aggregate model of A/C motors in a system, it is not accurate to model all the motors in the same manner. This would only reflect two modes of operation: all motors running and all motors stalled. From the analysis above, it is clear that there is a possibility of one motor running while the other motor is stalled. There is a possibility of cascaded motor stalling due to the stalling of one motor as well.

Chapter 4 Conclusions

A detailed dynamic load model for representation of the behavior of air conditioner compressor motors was presented in this thesis. The model is based on the dynamic phasor modeling approach and is sensitive to voltage and frequency. The model is simulated using the DAIS framework. The resulting motor speed, current, and power plots accurately capture the behavior of such machines during and after a fault. There are increasing numbers of FIDVR-type events being observed in the system and A/C motor stalling is found to be the primary reason for the occurrence of such events. Accurate A/C motor modeling is the key to properly identifying potential FIDVR events and designing appropriate mitigation plans to prevent reoccurrence of such events.

The added benefit of DAIS, which is the trajectory sensitivity information, is used to arrive at the more significant model parameters. This information may be used effectively in tuning the parameters for a large set of machines. The more significant model parameters according to the reactive power plot for different voltage tests are found to be: X_m , X_r , b_{sat} , X_c and n.

In order to develop an accurate composite load model, it is important to formulate a good methodology to aggregate a large number of A/C motors in the system. An analytical approach based on bifurcation theory is presented to develop such a methodology. A system consisting of an infinite bus connecting the load bus through a simple R-L network is considered. A continuation method based on the predictor-corrector approach is used to arrive at system steady-state solutions as the source voltage is varied. The plot of motor slip

vs source voltage shows all the possible operating regions possible: both motors running, one of the motors running while the other motor is stalled, and both the motors stalled. The simplified approach of aggregating all motors of similar rating into one equivalent motor would only reflect two possibilities: all motors running and all motors stalled. Also, the proposed approach shows the possibility of cascaded stalling of motors, depending on the system voltage and the inertia of the machines. This information may be crucial in developing mitigation plans to avoid a FIDVR event leading to a voltage collapse.

Future work could involve development of a composite load model that includes the phasor modeled A/C motor load suitable for system wide dynamic simulation studies. The results of the continuation method may be used for arriving at a more accurate aggregate motor model. The model may be eventually used for either detailed planning studies or for validation studies of other approaches to dynamic load modeling.

References

[1] B. Lesieutre, D. Kosterev and J. Undrill, "Phasor modeling approach for single phase A/C motors," *Proceedings of the IEEE PES General Meeting*, July 2008.

[2] J.W. Shaffer, "Air conditioner response to transmission faults," *IEEE Transactions on Power Systems*, vol. 12, no. 2, pp. 614-621, May 1997.

[3] B.R. Williams, W.R. Schmus and D.C. Dawson, "Transmission voltage recovery delayed by stalled air-conditioner compressors," *IEEE Transactions on Power Systems,* vol. 7, no. 3, pp. 1173-1181, August 1992.

[4] L. Taylor and S.M. Hsu, "Transmission voltage recovery following a fault event in the metro Atlanta area," *Proceedings of the IEEE PES Summer Meeting*, pp. 537-542, July 2000.

[5] I. Hiskens and M. Pai, "Trajectory sensitivity analysis of hybrid systems," *IEEE Transactions on Circuits and Systems I: Fundamental Theory and Applications*, Vol. 47, No. 2, pp. 204–220, February 2000.

[6] I. Hiskens, "Power system modeling for inverse problems," *IEEE Transactions on Circuits and Systems I: Regular Papers*, vol. 51, no. 3, pp. 539–551, March 2004.

[7] IEEE Task Force on Load Representation for Dynamic Performance, "Load representation for dynamic performance analysis," *IEEE Transactions on Power Systems*, vol. 8, no. 2, pp. 472-482, May 1993.

[8] C. Concordia and S. Ihara, "Load representation in power system stability studies," *IEEE Transactions on Power Apparatus and Systems*, vol. 101, no. 4, pp. 969-977, April 1982.

[9] L. M. Hajagos and B. Danai, "Laboratory measurements and models of modern loads and their effects on voltage stability studies," *IEEE Transactions on Power Systems*, vol. 13, no. 1, pp. 584-592, May 1998.

[10] S.J. Ranade, A. Ellis and J. Mechenbier, "The development of power system load models from measurements," *Proceedings of the IEEE PES T&D Conference*, October 2001.

[11] J.Y. Wen, L. Jiang, Q.H. Wu and S.J. Cheng, "Power system load modeling by learning based on system measurements," *IEEE Transactions on Power Delivery*, vol. 18, no. 2, pp. 364-371, April 2003.

[12] P. Ju, E. Handschin and D. Karlsson, "Nonlinear dynamic load modelling: model and parameter estimation," *IEEE Transactions on Power Systems*, vol. 11, no. 4, pp. 1689-1697, November 1996.

[13] Ma Da-Qiang and Ju Ping, "A novel approach to dynamic load modeling," *IEEE Transactions on Power Systems*, vol. 4, no. 2, May 1989.

[14] NERC Technical Reference Paper – Fault-Induced Delayed Voltage Recovery (FIDVR), June 2009.

[15] L.Y. Taylor, R.A. Jones and S.M. Halpin, "Development of load models for fault induced delayed voltage recovery dynamic studies," *Proceedings of the IEEE PES General Meeting*, July 2008.

[16] Vince Stewart and Ernst H. Camm "Modeling of stalled motor loads for power system short-term voltage stability analysis," *Proceedings of the IEEE PES General Meeting*, June 2005.

[17] P. Pourbeik and B. Agrawal, "A hybrid model for representing air-conditioner compressor motor behavior in power system studies," *Proceedings of the IEEE PES General Meeting*, July 2008.

[18] G. L. Chinn, "Modeling stalled induction motors," *Proceedings of the IEEE PES T&D Conference*, May 2006.

[19] D. Kosterev, A. Meklin, J. Undrill, B. Lesieutre, W. Price, D. Chassin, R. Bravo and S. Yang, "Load modeling in power system studies: WECC progress update," *Proceedings of the IEEE PES General Meeting*, July 2008.

[20] M.M. Abdel Hakim and G.J. Berg, "Dynamic single unit representation of induction motor groups," *IEEE Transactions on Power Apparatus and Systems*, vol. 95, no. 1, pp. 155-165, January 1976.

[21] C. A. Cañizares, "On bifurcations, voltage collapse and load modeling," *IEEE Transactions on Power Systems*, vol. 10, no. 1, pp. 512–522, February 1995.

[22] H. G. Kwatny, A.K. Pasrija and L. Y. Bahar, "Static bifurcations in electric power networks: loss of steady-state stability and voltage collapse," *IEEE Transactions on Circuits and Systems*, vol. 33, no. 10, pp. 981-991, October 1986.

[23] C. A. Cañizares, F. L. Alvarado, C. L. DeMarco, I. Dobson and W. F. Long, "Point of collapse methods applied to AC/DC power systems," *IEEE Transactions on Power Systems*, vol. 7, no. 2, pp. 673-683, May 1992.

[24] V. Ajjarapu and B. Lee, "Bifurcation theory and its application to nonlinear dynamical phenomena in an electrical power system," *IEEE Transactions on Power Systems*, vol. 7, no. 2, pp. 424-431, February 1992.

[25] J. S. T. Thorp, I. Dobson and H. D. Chiang, "A model of voltage collapse in electric power systems," *Proceedings of the IEEE Conference on Decision and Control*, vol. 3, pp. 2104–2109, December 1988.

[26] K. Iba, H. Suzuki, M. Egawa and T. Watanabe, "Calculation of critical loading condition with nose curve using homotopy continuation method," *IEEE Transactions on Power Systems*, vol. 6, no. 2, pp. 584-593, May 1991.

[27] V. Ajjarapu and C. Christy, "The continuation power flow: A tool for steady state voltage stability analysis," *IEEE Transactions on Power Systems*, vol. 7, no. 1, pp. 416-423, February 1992.

[28] A..J Flueck and W.Qiu, "A new technique for evaluating the severity of branch outage contingencies based on two-parameter continuation," *Proceedings of the IEEE PES General Meeting*, June 2004.

[29] N. Yorino, Li Hua-Qiang and H. Sasaki, "A predictor/corrector scheme for obtaining Q-limit points for power flow studies," *IEEE Transactions on Power Systems*, vol. 20, no. 1, pp. 130-137, February 2005.

[30] W.D. Rosehart and C.A. Cañizares, "Bifurcation analysis of various power system models," *International Journal of Electrical Power & Energy Systems*, vol. 21, no. 3, pp. 171-182, March 1999.

[31] C.D. Vournas and G.A. Manos, "Modelling of stalling motors during voltage stability studies," *IEEE Transactions on Power Systems*, vol. 13, no. 3, pp. 775–781, August 1998.

[32] "Voltage stability assessment: Concepts, practices and tools," IEEE PES Power System Stability Subcommittee, Technical Report SP101PSS, August 2002.

[33] V. Donde and I. Hiskens, "Shooting methods for locating grazing phenomena in hybrid systems," *International Journal of Bifurcation and Chaos*, vol. 16, no. 3, pp. 671-692, March 2006.